HHS Public Access

Author manuscript

Biomaterials. Author manuscript; available in PMC 2022 March 22.

Published in final edited form as:

Biomaterials. 2021 December ; 279: 121236. doi:10.1016/j.biomaterials.2021.121236.

A Src-H3 acetylation signaling axis integrates macrophage mechanosensation with inflammatory response

Praveen Krishna Veerasubramanian[a,b], **Hanjuan Shao**[a,b], **Vijaykumar S. Meli**[a,b], **Tri Andrew Q. Phan**[a,b], **Thuy U. Luu**[b,d], **Wendy F. Liu**[a,b,e,f,g], **Timothy L. Downing**[a,b,c,h,*]

[a]Department of Biomedical Engineering, University of California Irvine, Irvine, CA, USA

[b]UCI Edwards Lifesciences Foundation Cardiovascular Innovation and Research Center (CIRC), University of California Irvine, Irvine, CA, USA

[c]NSF-Simons Center for Multiscale Cell Fate Research, University of California Irvine, Irvine, CA, USA

[d]Department of Pharmacological Sciences, University of California Irvine, Irvine, CA, USA

[e]Department of Chemical and Biomolecular Engineering, University of California Irvine, Irvine, CA, USA

[f]Institute for Immunology, University of California Irvine, Irvine, CA, USA

[g]Department of Molecular Biology and Biochemistry, University of California Irvine, Irvine, CA, USA

[h]Department of Microbiology and Molecular Genetics, University of California Irvine, Irvine, CA, USA

Abstract

Macrophages are mechanosensitive cells that can exquisitely fine-tune their function in response to their microenvironment. While macrophage polarization results in concomitant changes in cell morphology and epigenetic reprogramming, how biophysically-induced signaling cascades contribute to gene regulatory programs that drive polarization remains unknown. We reveal a cytoskeleton-dependent Src-H3 acetylation (H3Ac) axis responsible for inflammation-associated histone hyperacetylation. Inflammatory stimuli caused increases in traction forces, Src activity and H3Ac marks in macrophages, accompanied by reduced cell elongation and motility.

*Corresponding author. 2408 Engineering Hall, University of California Irvine, CA, 92617, USA. tim.downing@uci.edu (T.L. Downing).

Credit author statement

P.K.V.: Methodology, Software, Validation, Formal analysis, Investigation, Data Curation, Writing - Original Draft, Visualization. H.S.: Investigation, Validation, Formal analysis. V.S.M.: Investigation, Validation, Formal analysis. T.A.Q.P.: Methodology, Software, Formal analysis. T.U.L.: Conceptualization, Investigation, Validation. W.F.L.: Conceptualization, Resources, Writing - Review & Editing, Supervision, Project administration, Funding acquisition. T.L.D.: Conceptualization, Resources, Writing - Review & Editing, Supervision, Project administration, Funding acquisition.

Declaration of competing interest

The authors have no competing interests to declare.

Appendix A. Supplementary data

Supplementary data to this article can be found online at https://doi.org/10.1016/j.biomaterials.2021.121236.

These effects were curtailed following disruption of H3Ac-signaling through either micropattern-induced cell elongation or inhibition of H3Ac readers (BRD proteins) directly. Src activation relieves the suppression of p300 histone acetyltransferase (HAT) activity by PKCδ. Furthermore, while inhibition of Src reduced p300 HAT activity and H3Ac marks globally, local H3Ac levels within the *Src* promoter were increased, suggesting H3Ac regulates Src levels through feedback. Together, our study reveals an adhesome-to-epigenome regulatory nexus underlying macrophage mechanosensation, where Src modulates H3Ac-associated epigenetic signaling as a means of tuning inflammatory gene activity and macrophage fate decisions in response to microenvironmental cues.

Keywords

Biophysical cues; Epigenetic regulation; Macrophages; Inflammation; Src-kinase signaling

1. Introduction

Macrophages play an important role in tissue healing and regeneration. A growing number of studies have demonstrated that these innate immune cells recognize extracellular mechanical cues that can consequently modulate their response to biochemical perturbations [1,2]. As mechanosensitive cells, macrophages respond to biophysical cues such as the extracellular matrix (ECM) architecture and composition, tissue stiffness, cell-cell contacts, fluid flow-mediated stretch, and compressive or shear forces [1]. These stimuli contribute to macrophage homeostatic function and also modulate their activation [3]. In particular, studies have demonstrated that the response of macrophages to proinflammatory cytokines is dampened within low-adhesive conditions where cells are, for example, patterned into confined [2] or elongated morphologies [4], or in contact with soft substrates [5]. Interestingly, more recent works have also demonstrated that macrophages generate differential extracellular forces in response to altered ECM stiffness and during classical pro-inflammatory (often referred to as M1) activation induced by bacterial lipopolysaccharide (LPS), which might further contribute to local tissue mechanics [6,7].

Cell shape alterations have been linked to several aspects of cellular function, including growth and apoptosis [8], differentiation and lineage commitment [9,10], and pathology [11,12]. *In vitro* observations show murine bone marrow derived macrophages (BMDM) undergo shape changes upon activation [4]. Inflammatory activation through LPS/IFNγ causes a flattening of adhered BMDMs, exhibiting a signature “fried-egg” morphology and causing a significant drop in the aspect ratio of the cells [4]. M2 activation (alternative activation, pro-wound healing) bestowed by the introduction of interleukins IL-4/IL-13 causes significant elongation of the macrophage population [4]. Such cell shape changes can also be triggered by mechanical changes within the cell microenvironment. For example, facilitated elongation of mouse BMDMs through the micropatterning of ECM proteins shows that elongated cells express higher M2 phenotypic markers even in the absence of polarizing exogenous cytokines [4]. Additionally, micropatterning macrophages enhanced the production of M2 marker Arginase upon IL-4/IL-13 treatment and reduced the expression of M1 marker iNOS post LPS/IFNγ exposure [4]. Other works observe a similar

effect when BMDMs were cultured on topographically grooved substrates, where cell elongation presents with reduced inflammatory tumor necrosis factor α (TNFα) secretion, and increased interleukin-10 (IL-10) and Arginase-1 production [13,14]. These observations have also been corroborated *in vivo* wherein implantation of biomaterials presenting grooved topographies elicited higher production of healing markers Arginase-1 and IL-10, compared to flat control materials [13].

Epigenetic gene regulatory mechanisms are key to both pro- and anti-inflammatory macrophage phenotypes [15]. Specifically, LPS-induced inflammation has been observed to enhance histone acetyl transferase (HAT) activity in BMDMs [16] and alveolar macrophages [17]. Moreover, several epigenetic drugs that either impede histone H3 acetylation (H3Ac) or their recognition by transcriptional complexes display anti-inflammatory effects [15]. Of considerable interest are the inhibitors of bromodomain and extraterminal domain (BET) proteins such as iBet762 [18] and JQ1 [19], which have substantial anti-inflammatory properties. Well-known members of the BET family of proteins include BRD2 and BRD4, both of which have been implicated in inflammation based on their localization to inflammatory gene promoters during macrophage polarization [19,20]. These H3Ac readers bind to relaxed regions of the chromatin marked by acetylated histones and act as scaffolds on euchromatin, facilitating binding by transcription elongation factors, transcriptional factors and other coactivators [21]. By supporting the stability and localization of protein complexes comprising inflammatory transcriptional factors such as NF-κB, STATs and IRFs, BET proteins contribute significantly to inflammatory program activation within macrophages [21].

Biophysically-induced cell shape changes have been known to modulate chromatin accessibility and control cellular behaviors such as reprogramming [22] and motility [23] through epigenetic histone modifications. In this study, we hypothesized that extracellular mechanical signaling alters inflammatory gene activity and macrophage fate decisions by tuning epigenetic regulation of transcription. We found that seeding macrophages on micropatterned (5 μm wide) fibronectin lines caused reduced expression of inflammatory markers such as *Nos2* and *Ccl2* when stimulated with LPS/IFNγ. These changes were concomitant with a reduction in bulk histone acetylation, and we sought a mechanism that would explain this observation. We found that Src and p300 HAT activity, both hallmarks of inflammatory activation, were suppressed in macrophages cultured on micropatterned lines. In addition, micropatterns induced similar cellular morphology and anti-inflammatory effects as soluble pharmacological BET inhibitors, and we explored these effects in parallel to identify their mechanistic intersections.

2. Materials and methods

2.1. Primary macrophage culture, activation and treatment conditions

BMDMs were cultivated and stimulated as previously described [4]. 8- to 12-week old female C57BL/6J mice (Jackson Laboratory) were sacrificed, and their femur and tibia dissected per Institutional for Animal Care and Use Committee (IACUC) approved protocols established at the University of California-Irvine. Subsequently, the bone marrow from each of the bones was flushed out and treated with ACK cell lysis buffer (Gibco). The cells

were then cultured in D10 media (DMEM with 10% fetal bovine serum (FBS), 100 U/mL Penicillin, 100 μg/mL Streptomycin, 292 μg/mL L-glutamine, all from Gibco) supplemented with recombinant murine macrophage colony stimulating factor (derived from CMG14-12/L929 cell supernatant) for 7 days on non-treated culture dishes. Day-7 cells were then seeded and allowed to adhere for 2 h (h) prior to stimulation. The macrophages were stimulated with 1 ng/mL of LPS (from *E. coli* O111:B4, Sigma Aldrich) and recombinant mouse IFNγ (R&D Systems) for 16 h resulting in macrophage inflammatory activation. Unstimulated cells were used as controls. iBet treatment, when used, was performed by introducing 1 μM of iBet762 (Sigma Aldrich) into the culture medium 30 min (min) prior to stimulation.

Gene knockdown were performed by electroporation using siRNA, 3 days prior to experiments (4D-Nucleofector, Lonza). BRD2 siRNA pool (GGAAAGGGCUCAUCGCCUA, CGGAAGCCCUACACUAUUA, GAAUUGGGAUCGAUGAAGA, GAGCUUGAGCGAUAUGUUU) (Horizon Discovery, Cat. M-043404-01-0005), and BRD4 siRNA pool (GAACCUCCCUGAUUACUAU, CAACAAACUUCCUGGUGAG, AAGGAAACCUCAAGCUGAA, ACAAUCAAGUCUAAACUAG) (Horizon Discovery, Cat. M-041493-00-0005) were both a mixture of 4 siRNA. Cytoskeletal inhibitors, when used, were also introduced 30 min pre-stimulation. Cytoskeletal inhibitors Cytochalasin-D (10 μM), Blebbistatin (30 μM), Y27632 (30 μM) and RKI-1447 (10 μM) were used at the indicated concentrations (all from Tocris Bioscience). Src inhibition and knockdown experiments were performed on cell seeded onto tissue culture plates. Src inhibitors PP1 (Cayman Chemicals) and PP2 (Millipore Sigma) were used at a concentration of 5 μM for a period of 6, 24 or 48 h. Src knockdown was performed using an siRNA pool (pool of 4 siRNA – UGACCGAGCUCACCACUAA, GGGAAACGGGCAAAUAUUU, GCACGGGACAGACCGGUUA, GCCAAGGGCCUAAAUGUGA) (Horizon Discovery, Cat. M-040877-01-0005), nucleofected at day 6 for a period of 48 h. A scrambled siRNA pool (UGGUUUACAUGUCGACUAA, UGGUUUACAUGUUGUGUGA, UGGUUUACAUGUUUUCUGA, UGGUUUACAUGUUUUCCUA) (Horizon Discovery, Cat. D-001810-10-05) was used for non-target controls. Cells were treated with rottlerin (5 μM, Tocris Bioscience) and curcumin (30 μM, Sigma) for 6 h before stimulation to inhibit the activity of PKCδ and p300 respectively.

After stimulation with 1 ng/ml of LPS and IFNγ, the cells were either fixed with 4% paraformaldehyde for immunostaining, lysed in Trizol (Sigma Aldrich) for qRT-PCR and NanoString gene expression profiling, or lysed in RIPA buffer (VWR) with protease and phosphatase inhibitor cocktail (Thermo Fisher) for proteins analysis through western blotting. The stimulation time course experiments in this study were performed using inflammatory stimuli concentrations of 10 ng/ml for LPS and IFNγ. A minimum of three individual biological replicate experiments were performed for all the analyses.

2.2. Micropatterning

Micropatterning was performed as described earlier [4]. In brief, silicon wafers with an array of 5 μm lines and 5 μm spacing was fabricated by standard photolithography and used

to create PDMS (1:10 ratio of resin base to crosslinker, Sylgard 184) stamps by replica molding (soft lithography). These stamps were washed with 70% ethanol and dried with a nitrogen gun, before being incubated with 20 μg/mL fibronectin for 1 h at room temperature (RT). PDMS spin-coated 25-mm coverslips were treated with UV Ozone (Jelight) and stamped onto with the fibronectin-coated PDMS stamps. The coverslips were then incubated in 0.2% (w/v) Pluronic F-127 (Sigma Aldrich) for 1 h at RT. The surfaces were washed with phosphate buffered saline (PBS) thrice before being seeded with cells at a density of 80,000 cells/mL. Flat controls were prepared by casting PDMS on 10 cm petri dishes and used for creating control unpatterned protein surfaces.

2.3. Cell migration and quantification

Cells were tracked via live-cell imaging of macrophages post stimulation for 12 h, with a capture frequency of 2 min. In brief, fibronectin was stamped onto PDMS-coated glass coverslips of dimensions 10 mm × 8 mm and transferred into glass bottom 8-chamber slides (Nunc Lab-Tek), before being blocked using Pluronic F-127 as described above. Cells were seeded at a density of 20,000 cells per well, and imaging was performed post stimulation. The images were processed to track the cell centroids using MTrackJ plug-in of Fiji [24]. The centroid data was analyzed using a custom python script. The metrics measured were: velocity – total distance traveled over unit time of observation, maximum displacement – the farthest distance traveled by a cell relative to its starting position, and mean square displacement (MSD) – average (over all observations) of the square of displacement. At least 40 cells per condition, from two biological replicates were analyzed.

2.4. Traction force microscopy (TFM)

Polyacrylamide (PA) gel substrates were prepared with a modified procedure of previously published protocols [25,26]. Briefly, glass coverslips (10 mm × 8 mm) were UV-ozone treated and functionalized using 0.3% (v/v) 3-(Trimethoxysilyl)propyl methacrylate (Sigma Aldrich) in 95% ethanol and 0.5% glacial acetic acid. Glass slides were functionalized with 0.1 mg/mL poly-D-lysine (Gibco) and a 1:800 (v/v) dilution of red fluorescent microspheres (0.5 μm carboxylate-modified, Thermo Fisher) in water [26]. A solution of 40% acrylamide and 2% bis-acrylamide (both Bio-Rad) was mixed to prepare 20 kPa gels [25]. Polymerization was initiated by the addition of 1:1000 (v/v) tetramethylethylenediamine and 1:100 (v/v) of a 1% ammonium persulfate solution (both Sigma Aldrich). 5 μL of PA solution was pipetted onto the functionalized glass slides and the functionalized glass coverslip was placed on top. After polymerization, the gels were peeled off, and fibronectin (20 μg/mL) was conjugated to the surface of gels with sulfo-SANPAH reagent (Thermo Fisher) [25]. The prepared PA gels were rinsed with PBS, and surfaced disinfected with UV light for 30 min, after which cells were seeded at 20,000 cells per well in glass bottom 8-chamber slides (Nunc Lab-Tek). Traction force microscopy imaging was performed by capturing images of microbeads and cell location at 2 h, 6 h and 15 h post stimulation. The cells were released from the gel surface with a 0.1% sodium dodecyl sulfate solution. Fiji software [24] was used to register any unaligned images. Subsequently, particle image velocimetry and Fourier transform traction cytometry were performed as previously described [27]. A custom code was written in Python and IJ1 macro language to batch process the single cell traction forces. While the estimated total elastic energy

is the integrated strain energy of the PA gel under elastic deformation by cell traction forces, the root-mean-squared (RMS) forces are calculated as the square root of the mean squared forces associated with the bead displacement by single cells, measured using 24 pixel interrogation windows as described before [6,28]. A minimum of 40 cells per condition from two biological replicates were analyzed.

2.5. RNA extraction, qRT-PCR and qPCR

RNA was extracted using Direct-zol RNA extraction kit (Zymo Research #R2051) and converted to cDNA using the High-Capacity cDNA Transcription Kit (Thermo Fischer Scientific #4368814). Reverse transcribed cDNA or genomic DNA from ChIP samples were used for quantitative PCR (qPCR). Samples were analyzed using SsoAdvanced™ Universal SYBR Green Supermix reagent (Bio-Rad #1725272). Primer concentrations were kept at 300 nM and 2 step qPCR was performed as described according to the manufacturer's protocol. The primers used for qRT-PCR and qPCR are attached in the supplement (Table S1).

2.6. Gene expression panel

Multiplexed gene expression analysis for 240 inflammatory genes was performed on macrophages undergoing stimulations on the flat (unpatterned) and micropatterned surfaces using the nCounter inflammation panel (NanoString Technologies). Samples from two biological replicate experiments were processed as recommended by the manufacturer. 2 h and 16 h LPS/IFNγ-treated cells were analyzed to understand differential gene expression at early and late time points. Data underwent background subtraction and filtering to eliminate lowly expressed genes, and was subsequently normalized to the geometric mean of six reference genes: *Cltc*, *Gapdh*, *Gusb*, *Hprt*, *Pgk1*, and *Tubb5*. Gene expression was also normalized to the positive controls in the panel. Genes that were expressed higher than two standard deviations above the mean of the negative background controls were selected for further analysis. Fold-change data were represented on a Log2 scale for both replicates and time-points.

2.7. Gene coregulation network analyses

Gene correlation analysis was performed using gene expression data (GEO Number: GSE21764) from BMDMs stimulated for 1, 2, or 4 h with LPS and with or without iBet treatment. Pearson's correlation coefficients for all pairwise arrangements were calculated for the inflammatory genes that showed over 1.5-fold change in micropatterned vs. flat surfaces (averaged across two biological replicates) in our gene expression dataset, as well as LPS-sensitive integrin and cadherin genes (from the adhesome gene sets in Refs. [29–31]). A correlation threshold of 0.9 was set for the adjacency matrix. Gene nodes without any correlation were excluded. The correlation network was visualized using the igraph package in R [32]. Protein-protein interactions in this study were mapped using the String database [33].

2.8. ChIP-seq data mining

H3Ac enrichment data were obtained from ChIP-Seq experiments from a separate published study (GEO: GSE21910) [18]. H3Ac enrichment was measured for the genes in the gene correlation network described above. H3Ac binding was quantified as a summation of enrichment above a background threshold, in the promoter regions defined by 10 kilobases centered around the start of each gene. The enrichment data were converted to Z-scores for visualization as a heatmap for annotation of the gene correlation network described above.

2.9. Immunostaining, western blots and ELISA

Cells were fixed with 4% paraformaldehyde (EMS), and permeabilized with 0.3% Triton X-100 (Sigma Aldrich) in PBS with a 10 min incubation. Primary antibody, against either integrin αV/β3 (1:200 (v/v), Novus Biologicals, Cat. SC56-07), H3Ac (1:500 (v/v), Millipore Sigma, Cat. 06–599), iNOS (1:50 (v/v), Abcam, Cat. 15323), NF-κB (1:200 (v/v), Santa Cruz, Cat. sc-8008), or Src (1:500 (v/v), Cell Signaling, Cat. 2108) was used overnight at 4 °C. After 3 h of incubation at RT with Alexa Fluor 594 conjugated secondary antibody (Abcam), cells were incubated for 30 min with Alexa Fluor 488-Phalloidin and DAPI (both Life Technologies). The samples were then mounted with fluoromount-G (Southern Biotech) for visualization using a confocal microscope (Zeiss LSM780 or Olympus Fluoview FV3000). Staining for vinculin/focal adhesion kinase were performed using a staining kit (Sigma, Cat. FAK100) following the manufacturer's instructions. For western blotting, SDS-PAGE was performed using 4–15% gels (Bio-Rad) at 70 V, and the proteins were transferred using a dry blot transfer system to nitrocellulose membranes (iBlot2). The blot was blocked with 5% bovine serum albumin (BSA) and probed overnight at 4 °C with either H3Ac (1:1000 (v/v), Millipore Sigma, Cat. 06–599), Src (1:1000 (v/v), Cell Signaling, Cat. 2108), phospho Src (Y416) antibody (1:1000 (v/v), Cell Signaling, Cat. 6943), phospho PKCδ (Y311) (1:1000 (v/v), Cell Signaling, Cat. 2055), PKCδ (1:1000 (v/v), Abcam, Cat. ab182126), phospho STAT1 (Y701) (1:1000 (v/v), Cell Signaling, Cat. 9167), STAT1 (1:1000 (v/v), Cell Signaling, Cat. 14994), or HIF1α (1:1000 (v/v), Cell Signaling, Cat. 36169) primary antibody followed by incubation with an anti-rabbit IgG HRP secondary antibody (1:2000 (v/v), Cell Signaling) at RT for an hour. GAPDH (1:2000, Santa Cruz, Cat. sc-59540) was used to normalize the cell lysate loading. ELISA was performed as per standard techniques using a mouse MCP-1 kit (Biolegend, Cat. 432704).

2.10. Cytokine profiling

Cytokine profiles for macrophage response to LPS/IFNγ with inhibitory drug treatments were probed by multiplexed analyte analysis (Mouse Cytokine Array/Chemokine Array 31-Plex (MD31), Eve Technologies, Calgary, CAN).

2.11. Chromatin immunoprecipitation followed by qPCR (ChIP-qPCR)

ChIP experiments were performed using previously established methods [34]. Flat and micropatterned surfaces were created on 150 mm PDMS-coated petri dishes onto which 5 million cells were plated for each of the conditions. After 2 h of stimulation, culture media was aspirated out and the cells were crosslinked with 1% paraformaldehyde (EMS) for 10 min at RT. The fixation was quenched with the addition of 0.125 M glycine in PBS for 5

min and cells were scrapped into cell lysis buffer (0.5% Nonidet-40 and 85 mM KCl in 20 mM Tris-HCl, pH 8.0). Nuclei were pelleted at 2500×*g* for 5 min, and then lysed with nuclei lysis buffer (0.1% sodium dodecyl sulfate, 0.5% sodium deoxycholate, 1% Nonidet-40 in 10 mM Tris-HCl, pH 7.5). Chromatin from the nuclear lysate was then sheared for 8 min (0.7 s on and 1.3 s off pulses) using a probe sonicator (Branson Sonifier SFX250) at 40% amplitude. All steps were performed on ice. Approximately 10 μg of chromatin was used per immunoprecipitation with 2 μg of H3Ac antibody (Millipore Sigma, Cat. 06–599) at 4 °C overnight. The precipitates were recovered with magnetic protein A/G beads (Thermo Fisher), and washed twice serially with low salt immunocomplex buffer, high salt immunocomplex buffer, lithium chloride immunocomplex wash buffer, and Tris-EDTA (pH 8). Immunoprecipitated protein-DNA complexes were eluted into a solution of 1% SDS and 100 mM sodium bicarbonate, and then reverse crosslinked overnight at 65 °C in a solution containing RNase A and proteinase K. The DNA was recovered using AMPure XP magnetic beads (Beckman Coulter), washed with 70% ethanol, and then quantified by qPCR. DNA enrichment has been represented as the fraction of input and is presented as fold versus H3Ac binding in macrophages cultured on flats.

2.12. HAT activity assay

Total HAT activity was measured using a colorimetric kit (Epigentek, Cat. P-4003-96), following the manufacturer's recommended protocol. Nuclear extracts from 5×10^6 cells collected 2 h after LPS/IFNγ stimulation were isolated using the methods described above for ChIP-qPCR. p300 HAT activity was measured using the same assay techniques, except that p300 was immunoprecipitated [35] using a p300 antibody (Abcam Cat. ab10485, 1:100 (v/v)) overnight and purified using magnetic protein A/G bead before the HAT assay.

2.13. Image analysis

Analyses of cell morphology and quantification of fluorescent intensity were performed using Fiji software [24]. Cell morphology was ascertained by demarcating the outlines of phalloidin stained cells manually. DAPI-stained nuclei were used as masks for nuclear intensity quantification of the protein/channel of interest, and the integrated intensity of protein fluorescence in the nucleus was assessed on a per-cell basis. A minimum of 60 cells were analyzed from replicate experiments.

2.14. Data acquisition and mining

Data represented in this manuscript (specifically Fig. 1c–f, 3a and 7cd) had been collected as part of a published doctoral dissertation at UCI [36]. Data were also mined from publicly available microarray (GEO Number: GSE21764) and ChIP-Seq datasets (GEO: GSE21910) [18]. Previously curated adhesome gene sets that described the components of the integrin and cadherin networks were used for analysis [29–31].

2.15. Statistical analysis

One-way ANOVA with multiple comparisons using Tukey test were performed on GraphPad Prism (v8, GraphPad software). The same software was used to perform Student's t-test in

experiments where there were only two treatment groups. Data are represented as mean ± SEM in the bar plots. Median and quartiles have been marked in the violin plots.

3. Results

3.1. BET inhibition and facilitated cell elongation prevent inflammation-associated cell rounding and gene expression

To assess the effects of inflammation on cell shape, we activated macrophages cultured on flat control substrates with 1 ng/ml LPS/IFNγ. Unstimulated macrophage populations appeared as a mixture of elongated and, occasional, circular cells. LPS/IFNγ treatment caused cytoskeletal flattening and rounding, thereby significantly reducing the cell aspect ratio (Fig. 1b,d) [4]. We used micropatterning to facilitate cell elongation on 5 μm wide fibronectin lines, while keeping unpatterned, flat stamped surfaces as a control (Fig. 1a and b). Macrophages display an elongated morphology on micropatterned surfaces in both unstimulated and LPS/IFNγ-treated conditions, demonstrating the abrogation of shape changes associated with the M1 phenotype (Fig. 1b,d). Interestingly, the disruption of H3Ac readers by iBet762 (henceforth described as iBet) and JQ1 also caused most of the population to retain an elongated morphology even with LPS/IFNγ stimulation (Figs. 1b and S1a). In addition, we observed that inflammatory genes responsible for free radical production (*Nos2*) and macrophage recruitment (*Ccl2*) were both downregulated in macrophages with BET inhibition and micropattern-facilitated elongation (Fig. 1c).

Quantification of the nuclear aspect ratio and two-dimensional projected area revealed a notable change with LPS/IFNγ activation (Fig. 1e and f). LPS/IFNγ stimulation caused rounding of nuclei within the cell population while increasing the nuclear area, without altering nuclear volume (Fig. 1g). Interestingly, while the micropatterned cells resist the rounding and flattening of nuclei that typically occurs with LPS/IFNγ stimulus, iBet treatment did not prevent inflammation-associated shape changes within nuclei (Fig. 1f). However, the nuclear volume was significantly lower with micropatterning and iBet treatment, pointing to a more compact nucleus (Fig. 1g). BET inhibition using JQ1 causes morphological changes identical to that of iBET treatment (Figs. S1b–d), further confirming that cellular elongation was likely caused by BET inhibition. Silencing both *BRD2* and *BRD4* suppresses inflammatory markers *Ccl2* and *Nos2*, and abrogates the inflammatory stimulation-induced circularization of cells (Fig. 1h and i). Together, these observations on morphology and gene expression suggest that altered inflammatory states in macrophages might be coordinated through both BET signaling and cell shape changes.

3.2. Cellular elongation alters adhesive structures

Our analysis of adhesome genes in macrophages over time demonstrate the dynamic expression of cytoskeleton and associated genes with inflammatory polarization (Fig. S5). Such a dynamic adhesome [1,37] is suggestive of an altered mechanical state in response to LPS/IFNγ stimulation that can explain cell shape-related morphological observations. Based on this, we hypothesized that the micropatterning induced macrophage elongation causes differential regulation of cell adhesive structures. Given that the fibronectin-binding integrin $\alpha_v\beta_3$ is involved in cell-substrate engagement and guided cellular behavior like migratory

persistence [38], we examined its expression by staining. In agreement with our previous report [39], we find that integrin $\alpha_v\beta_3$ was lower expressed in cells that were stimulated with LPS/IFNγ (Fig. S2). Interestingly, treatment with iBet or elongation along micropatterns caused higher integrin $\alpha_v\beta_3$ expression, although this is not necessarily indicative of higher integrin engagement. Therefore, we also visualized focal adhesions by staining vinculin. On the micropatterns and in cells treated with iBet, vinculin staining was more diffuse and lower overall (Fig. 2a), suggesting that adhesive interactions may be repressed in elongated cells [14]. Given these results, we next explored the possibility of alterations in motility and traction forces caused by such disruptions to adhesive structures.

3.3. Cellular elongation correlates with increased motility

Cell motility is a hallmark of macrophages and a critical attribute for carrying out their functions of innate immunity. Cell motility across control, iBet-treated, and micropatterned conditions showed no significant differences across all metrics of motility measured (displacement and velocity) in the absence of stimulation. We noted that, as previously reported [7,39], LPS/IFNγ-activated BMDMs exhibited a reduced propensity for migration relative to unstimulated cells (Fig. 2b–e). BET inhibition protected activated macrophages from this inflammation-associated reduction in motility, as motility metrics remained elevated in iBet-treated cells relative to untreated cells upon LPS/IFNγ treatment (Fig. 2b–e). We observe similar trends in cells that were micropatterned. Inflammatory stimuli did significantly reduce migration speed on patterns, however cells cultured on patterns still tended to migrate farther and faster than stimulated cells on flat surfaces. These data suggest that modulation of macrophage motility through use of micropatterned substrates or iBet treatment is coordinated with macrophage shape and phenotype.

3.4. BET inhibition in macrophages prevents the upregulation of cell traction forces during stimulation with LPS/IFNγ

Our analysis of morphology revealed a sizable proportion of iBet-treated cells presenting increased leading-edge like protrusions (i.e. greater than 2) that were rapidly formed and dissipated (Fig. 2g). These transient lamellipodia/filopodia-like appendages, were observed in actively migrating cells and could be involved in mechanosensation [40]. Macrophage motility has been previously described as being driven by frontal-towing, where the force generated by the migrating cell is concentrated in its leading edge [6]. Since traction and adhesive forces drive cell motility, we sought to see if there existed differential traction forces in iBet-treated cells. LPS/IFNγ-mediated polarization of macrophages resulted in an increase in root-mean-squared (RMS) traction forces (Fig. 2f) up to 15 h post LPS/IFNγ addition. These heightened traction forces were dampened in the presence of iBet, which corroborates our observations of reduced motility in iBet-treated cells. Traction forces are often attributed to cell shape changes [41], among other factors. Thus, this increase in traction forces could potentially explain the flattening of macrophages in response to inflammatory stimuli.

3.5. Micropattern-elongated and iBet-treated macrophages display largely divergent responses to inflammatory stimulation

To gain a better molecular understanding of the inflammatory gene suppression that occurs when macrophages cultured on micropatterned surfaces are subjected to LPS/IFNγ stimulus, we utilized a multiplexed inflammatory gene analysis panel. We were able to ascertain that patterned surfaces modulate inflammatory gene expression after as little as 2 h of an inflammatory stimulus (Fig. 3a). However, such differential expression is more apparent after 16 h of stimulation, where there is a significant downregulation of canonical inflammatory makers, such as *Nos2* and *Ccl2*. Unexpectedly, we also find that our patterned surfaces upregulate the expression of *Nfkb1* (pro-inflammatory transcription factor NF-κB) along with a number of other genes in this inflammatory panel. Comparing these data with the documented effects of iBet (GEO: GSE21764 [18]), we find that very few genes that were upregulated by the patterned surfaces experience similar changes with iBet treatment. These discrepancies in gene regulation could be due to fact that iBet globally targets (and competitively inhibits) BET proteins, which are epigenetic readers of H3Ac that are involved in gene activation, while the pathways affected by patterned surfaces may have a more nuanced impact on gene regulation at specific targets.

3.6. Elongation-induced dynamic inflammatory genes are strongly coregulated with adhesome genes dynamically regulated during polarization

To further investigate the relationship between biophysically-altered gene regulation in macrophages and the H3Ac epigenetic landscape, we leveraged temporal gene expression data of polarized macrophage from the previously mentioned dataset [18] to build a gene expression coregulation network of genes involved in inflammation and macrophage mechanoregulation. To do so, we first included inflammatory genes that we observed to by dynamically regulated by patterned surfaces from our NanoString data (Fig. 3a). Given that we have previously observed that monocyte differentiation into macrophages and subsequent LPS stimulation lead to dynamic expression levels in the genes which encode for proteins involved in cell-ECM and cell-cell contact-mediated forces [1] (described by others as the integrin and cadherin adhesomes, respectively [29–31]), we added LPS-sensitive adhesome genes to our network analysis. By building this network using LPS-sensitive adhesome genes and the inflammatory genes that were differentially regulated by patterned surfaces, we observe a notable relationship between the expression of several adhesome and inflammatory genes (Fig. 3b). The network shows a strong correlation between inflammatory and adhesome genes, suggesting that these genes may be coregulated in response to LPS-treatment (Fig. 3b,f). While the number of positive correlations per gene is roughly the same for both inflammatory and adhesome genes, it was interesting that the adhesome genes displayed nearly double the number of negative correlations compared to the inflammatory genes (Fig. 3b). In addition, there existed a sizable proportion of both positive and negative correlations between adhesome and inflammatory gene network connections (Figs. 3d and S3a). This points towards a strong coregulation of inflammatory and adhesome genes with inflammatory polarization. Mapping the protein-protein interactions using the tools from String database [33], we find that several of the adhesome and inflammatory genes under consideration have been reported to be associated on a protein level as well (Fig. S3b). Particularly noteworthy is Src (an adhesome gene

that was highly correlated in our coregulation network) which has been reported to have protein-level interactions with several inflammatory and adhesome genes, placing it at the interface of several adhesome to inflammatory signaling cascades (Fig. S3b).

3.7. H3Ac levels at coregulated gene promoters are dynamic upon stimulation

Following the creation of our gene correlation network, we sought to identify potential epigenetic regulatory mechanisms that might explain such coordination in adhesome and inflammatory gene regulation. To accomplish this goal, we performed a differential enrichment analysis on a previously existing ChIP-seq dataset (probed for H3Ac peaks) in primary mouse macrophages stimulated with LPS, with or without iBet treatment (GEO: GSE21910) [18]. From this analysis, we identify genes from our correlation network whose promoters exhibit changes in H3Ac enrichment following LPS stimulation. We were also able to identify promoters whose H3Ac levels were dependent on BET signaling (e.g., those that were altered by iBet exposure). We used this analysis to cluster genes according to promoter H3Ac enrichments and identify trends in the dynamic relationship between promoter H3Ac and gene expression across experimental conditions (Fig. 3c). Accordingly, cluster 1 comprised genes whose H3Ac enrichment within their promoter region was maintained with LPS-treatment, but still sensitive to iBet. Cluster 2 contained genes with reduced H3Ac enrichment upon inflammatory stimulation, and that were potentially sensitive to additional losses in H3Ac by iBet treatment. We found that most of the negative gene correlations in the network involved genes of cluster 2, irrespective of whether the correlation was an inter- or intra-cluster (Fig. 3e). The intra-cluster correlations between the genes belonging to cluster 1 were majorly positive (96%), suggesting a high degree of coexpression in the genes of this cluster in response to LPS treatment. In addition, a significant number of adhesome genes within cluster 1 correlated tightly with a vast majority of genes in the network, explaining their prominent presence at the center of the network. To better highlight the relationship between each cluster category and the genes within our coregulation network, we have added this annotation to our network (Fig. 3b). Since the clusters were fundamentally different in their H3Ac dynamics, this observation suggested that epigenetic regulatory mechanisms through promoter H3Ac in response to LPS could be responsible for at least some of the inflammation-associated adhesome gene changes. In addition, these observations support the existence of co-regulatory mechanisms of inflammatory and adhesome gene expression through epigenetic means, although further studies would be necessary to establish more definitive proof of such mechanisms.

3.8. Cytoskeletal disruption impedes inflammation-associated histone hyperacetylation

The ChIP-seq analysis suggested a highly dynamic H3Ac state in the first hours of inflammatory stimulation. Hence, we wished to characterize changes to global H3Ac levels resulting from LPS/IFNγ stimulation. Staining for H3Ac, we noted a surge in the total H3Ac levels in cells polarized with LPS/IFNγ (Fig. 3g). Furthermore, we observed that macrophages treated with cytoskeletal inhibitors targeting the actomyosin network displayed lower H3Ac levels, even with activating stimuli. These findings suggest that biomechanical forces and other signaling events translated through the cytoskeleton may be instrumental to the observed rise in H3Ac levels in response to LPS/IFNγ activation. From our gene coregulation analysis, ChIP-seq mining and reported protein-protein interactions,

we narrowed our search for an LPS- and iBet-sensitive adhesome component that potentially modulated H3Ac levels down to the signaling kinase Src.

3.9. Src expression and activity is essential for inflammatory histone hyperacetylation

Since Src emerged as a promising candidate pivotal to a putative mechanosensory-inflammatory H3Ac axis, we hypothesized that Src signaling was involved in histone H3 hyperacetylation in macrophages. To test this, we knocked down Src using a siRNA pool. We confirmed Src depletion at 48 h by quantifying both mRNA and protein expression (Figs. S6a and b). siSrc treatment results in reduced inflammatory expression of iNOS and MCP-1 (Fig. 4a and b), and also of their respective mRNA transcripts *Nos2* and *Ccl2* (Fig. 4c). Notably, siSrc treatment caused a reduction in bulk H3Ac levels in unstimulated (Fig. 4d) and LPS/IFNγ-stimulated (Fig. 4e) cells. Next, we wanted to explore the possibility of Src controlling H3Ac levels by modulating histone acetyltransferase (HAT) activity. We found that total HAT activity increases in control macrophages when treated with LPS/IFNγ - possibly due to inflammatory programs requiring an increase in the accessibility of inflammation-specific genes [42]. Src depletion results in an about 20% reduction in total HAT activity (Fig. 4f). Src depletion also impaired the inflammation-associated surge in HAT activity that was observed in control condition. Since p300 is an important HAT associated with macrophage inflammation [15,42], we also measured p300 HAT activity by coupling immunoprecipitation techniques with HAT activity assays. We find that p300 HAT activity is increased by about 50% with inflammatory activation. siSrc treatment causes a significant decrease in p300 HAT activity in cells stimulated with LPS/IFNγ, and these p300 activity levels were comparable to those observed in unstimulated cells. This suggested that the global increase in H3Ac levels that are triggered during inflammatory activation is orchestrated by Src-dependent p300 HAT activity.

Earlier studies have shown that not only do Src levels increase with inflammation, but Src also gets activated by phosphorylation of residue Y416 upon inflammatory polarization [43]. We utilized Src pharmacologic inhibitors PP1 and PP2 to curb the activation of Src at the protein level, and found that both of these inhibitors significantly impaired Src phosphorylation (Figs. 5a and S7a). Src inhibition caused dampened iNOS expression (Fig. 5d) and MCP-1 production (Fig. 5b) by macrophages exposed to LPS/IFNγ. This also corroborates with the lower *Ccl2* and *Nos2* gene expression observed with Src inhibition (Figs. 5c and S7b). PP1/2-mediated Src inhibition also results in lower H3Ac levels in both resting (Figs. 5e and S7c) and LPS/IFNγ-treated cells (Fig. 5f). We also measured p300 HAT activity with PP1 and PP2 treatments. Both drugs suppressed LPS/IFNγ-associated increases in p300 HAT activity, further demonstrating that Src activation is responsible for inflammatory histone hyperacetylation and p300 HAT activity (Fig. 5g). Since Src inhibition resulted in diminished *Ccl2* expression, we sought to test if this can be explained through changes to H3Ac locally at the *Ccl2* proximal promoter. PP1 and PP2 treatments caused significant reductions in H3Ac enrichment at the *Ccl2* promoter in unstimulated cells, and marginal drops in LPS/IFNγ-treated cells (Fig. 5h).

Interestingly, we observe that inhibiting Src activity using PP1 and PP2 results in elevated promoter H3Ac enrichment in inflammatory polarized cells (Fig. 5i). There is also a

corresponding increase in *Src* transcript levels in the cells treated with Src inhibitors (Fig. 5j). This is suggestive of a regulatory compensation mechanism involving negative feedback that makes it possible for cells to withstand sufficient levels of Src activity during inflammatory stimulation.

3.10. PKCδ links Src activation with elevated p300 HAT activity

While the influence of Src on p300 HAT activity and H3Ac levels were evident from our results, we sought a mechanism by which Src could impact p300. In our literature search, we came across protein kinase C delta (PKCδ), a kinase that contributes to inflammation in macrophages and has been reported to rein in p300 HAT activity by phosphorylation within some *in vitro* systems [44]. In addition, the activation of Src kinase has been shown to phosphorylate PKCδ at Y311 which suppresses its activation by caspase-mediated cleavage in 3T3 fibroblasts [45]. Y311 phosphorylation of PKCδ also results in its potential ubiquitination and degradation [45,46]. We wished to explore the possibility that Src activation leads to an increase in p300 HAT activity and histone hyperacetylation by suppressing PKCδ, and explore the relevance of such a mechanism in the macrophage inflammatory process.

To answer this, we first performed an LPS/IFNγ stimulation time course, exploring changes in Src activation, histone acetylation and PKCδ levels (Fig. 6a). We found that Y416 phosphorylated Src increased within the first 15 min of inflammatory stimulation and the levels remained heightened for the duration of our time course (360 min). Histone acetylation was also seen to increase quickly, and was significantly higher at the 60-min time point, which coincided with the start of transcriptional activity of factors such as NF-κB. This increase in H3Ac levels was sustained for up to at least 360 min (data not shown). Interestingly, Y311 phosphorylated PKCδ increased transiently, with an abrupt decay beginning around 90 min after the onset of stimulation. This also coincided with a transient drop in total PKCδ levels, that return to pre-stimulation levels. Based on previous reports that p300 HAT activity is suppressed by PKCδ [35,44], we posited that p300 activity is freed from suppression by PKCδ as a result of Src activation upon inflammatory polarization.

To study the effects of Src, PKCδ, and p300 on macrophage inflammatory activation, we blocked the activity of these molecules with PP1/PP2, rottlerin and curcumin, respectively, and profiled cytokine secretion (Fig. 6b). We found that blocking p300 had significant anti-inflammatory outcomes including a reduced IL-6, TNFα, and MCP-1 production. PP1 was overall anti-inflammatory, and along with PP2 caused a decreased MCP-1 production by the cells. The impact of rottlerin was mixed, as it both upregulated and downregulated some inflammatory genes. We also studied the impact of these drugs on transcriptional factors such as NF-κB, STAT1 and HIF-1α. We find that curcumin reduces total NF-κB levels in both unstimulated and LPS/IFNγ stimulated cells (Fig. S8b). Inflammation-induced STAT1 activation, which is marked by an increase in Y701 phosphorylated STAT1, is blocked in cells treated with rottlerin (Fig. S8a), potentially explaining some of the anti-inflammatory effects of rottlerin observed within our cytokine secretion profiles. HIF-1α, whose levels increase with inflammation as a result of stabilization, are suppressed in the absence of Src

activation, as seen in both PP1 and PP2 treated cells (Fig. S8a). These results underline the effects of each of these molecules in macrophage inflammation.

Our next experiment examined the effects of rottlerin and curcumin on bulk H3Ac levels (Fig. 6c). As expected, our p300 inhibitor curcumin led to a drastic drop in H3Ac expression, while rottlerin caused an increase in H3Ac levels. These results can be explained by the opposing impacts that these drugs have on p300 HAT activity – e.g., curcumin induced a precipitous drop in p300 HAT activity, while rottlerin caused an increase in p300 activity in both unstimulated and stimulated cells (Fig. 6d). These results demonstrate that suppression of PKCδ can activate p300 HAT activity and lead to histone hyperacetylation.

We next wished to test the hypothesis that Src inactivation relieves PKCδ suppression and degradation. Observing total PKCδ and Y311 phosphorylated PKCδ levels in cells treated with PP1 and PP2 at 1-h post-stimulation, we observe that PP1 and PP2 treatments reduce Y311 phosphorylation of PKCδ, and diminish the transient drop in PKCδ levels (Fig. 6e). These results show that Src activation post-stimulation is indeed necessary for the suppression and degradation of PKCδ.

3.11. Micropatterned-induced macrophage elongation reduces global and local histone acetylation

Based on our observation that Src activation and subsequent PKCδ suppression was necessary for p300-mediated H3 hyperacetylation, we wished to observe *Src* expression and activation in iBet-treated and micropatterned (elongated) cells. We found that iBet treatment causes downregulation of *Src* gene expression as expected (Fig. 7a, Fig. S5) [18]. However, *Src* levels in micropatterned cells were unchanged in both unstimulated and LPS/IFNγ-treated comparisons. We next wanted to observe if Src activation was hampered in the elongated cells. By measuring the ratio of phospho-Src (Y416) to total Src using western blots, we observe that there is an increase in Src activation upon LPS/IFNγ stimulation as expected [43]. However, phospho-Src levels do not increase significantly on micropatterned cells (Fig. 7b). This suggests that adhesome rearrangements induced by cellular elongation hamper Src activation by inflammatory stimulus, but do not trigger upregulation of *Src* expression as previously observed during pharmacological inhibition of Src activity through PP1/PP2 on flat surfaces (Fig. 5i and j).

Previous studies had noted that cellular elongation changes H3Ac level in fibroblasts and mesenchymal stem cells [22,47]. We wished to ascertain if total H3Ac levels varied with the elongation of macrophages. We noticed with both western blotting and immunofluorescence imaging that micropatterned cells exhibited lower global H3Ac marks (Fig. 7c and d). We also observed reduced total HAT and p300 HAT enzymatic activity in macrophages on micropatterns that were treated with inflammatory stimulus (Fig. 7e), corroborating with the reduced bulk H3Ac levels.

We further postulated that global reduction in H3Ac on micropatterns would translate to decreased levels of H3Ac at inflammatory gene promoters. ChIP-qPCR analysis showed significant drops in H3Ac enrichment at *Ccl2* and *Src* promoter regions of micropatterned cells compared to unpatterned cells (Fig. 7f). We also observe reduced H3Ac enrichment

at the promoter of *Cd86* (an pro-inflammatory macrophage marker), and unchanged H3Ac levels at the *Mrc1* (an anti-inflammatory marker) gene promoter in unstimulated micropatterned cells.

4. Discussion

Many studies have focused on cell shape associated phenotypic changes, and their relationship with altered epigenetic states. One such study found that cellular elongation and spreading correlate with nuclear deformation and orientation [48]. Furthermore, elongated cells also exhibited significantly higher chromatin condensation and cell proliferation [48]. Elongation of mesenchymal stem cells by micro-topography or mechanical stretch causes increased nuclear elongation, and differential histone 3 acetylation (H3Ac) and histone modifying enzyme activity [47]. The biophysical regulation of osteogenic differentiation [49] and cell reprogramming [22] are also associated with changes in the epigenetic landscape. In mammary epithelial cells, it was reported that disruption of the actin cytoskeleton caused histone deacetylation [50]. Furthermore, the morphology of macrophages is known to correlate with their molecular phenotype *in vivo*. For instance, elongated macrophages found within atherosclerotic lesions of coronary arteries, a microenvironment that exhibits abnormal biomechanical cues, express CD68 and CD14 while rounded macrophages express CD68 only [51]. With these in mind, we asked if similar forms of biophysically induced epigenetic modulation can explain the altered inflammatory response commonly observed in elongated macrophages [4].

In this study, we revealed altered epigenetic states and inflammatory gene expression profiles that arise alongside the elongation of macrophages and compared these altered molecular signatures with those induce through inhibition of BET (H3Ac reader) epigenetic signaling. Notably, we found that, similar to micropatterned and alternatively activated macrophages [4], iBet treatment promoted a more elongated cell morphology along with a suppressed inflammatory response. This morphological and inflammatory suppression of macrophage response to LPS/IFNγ was also reproduced in *BRD2* and *BRD4* deficient cells, showing that these specific BRD proteins play a role in guiding macrophage inflammation. Furthermore, we found that, in addition to canonical alteration in cellular shape, macrophages also increased the magnitude of their ECM traction forces upon inflammatory stimulation (with LPS/IFNγ addition), which led to concomitant reductions in migratory potential (speed and maximum displacement). This suggests that increased traction forces in inflamed cells may be utilized to increase ECM anchorages in order to reduce cell mobility. These effects on migration and traction force were also subdued in the presence of iBet, and cells cultured on low-adhesive micropatterned surfaces also retained significantly higher migratory potential. Taken together, these findings more closely connect cell-mediated force generation and the migratory potential of macrophages, which are undoubtably influenced by properties of the local microenvironment, to the expression of proinflammatory cytokines, including those involved in the recruitment of additional macrophages into the local tissue environment (e.g., MCP-1) to facilitate critical functions of innate immunity. These findings also corroborate a number of recent studies highlighting the importance of heightened cytoskeleton tension in macrophage polarization [52–54], where the acquisition of an inflammatory state requires cytoskeletal tensions large enough to

facilitate the nuclear shuttling of key mechanotransducers (e.g., YAP/TAZ [5] or MRTF [2]) and activation of mechanically-gated ion channels (e.g., Piezo1) [55].

While elongated macrophages expressed lower levels of classical M1 markers and inflammation-associated cellular and nuclear shape changes, an analysis of 240 inflammatory genes reveals that the impacts of facilitated macrophage elongation on LPS/IFNγ treatment are not classifiable as purely pro- or anti-inflammatory. This was in stark contrast to the effects of iBet, which largely suppressed pro-inflammatory (M1) marker expression. However, the relationship between cell shape, motility and traction forces as macrophages polarize with LPS/IFNγ stimulation were also substantiated by examining the effect of polarization on adhesion and motility related genes. Specifically, reanalysis of existing datasets revealed that LPS stimulation caused sweeping changes in adhesome gene expression levels, possibly to further support alterations in morphology and migratory behavior (Figs. S4 and S5). Additionally, we noted a multifaceted relationship between adhesome and inflammatory gene expression using gene correlation network analysis. Intriguingly, iBet treatment partially blocks the incidence of inflammation-associated changes in adhesome and inflammatory gene expression, potentially explaining the persistence of cellular elongation even in the presence of inflammatory stimulus (Figs. S4 and S5). This also suggested that epigenetic regulatory mechanisms involving H3 acetylation may influence the co-regulation of inflammatory and adhesome genes during inflammatory stimulation.

Acetylation of lysine residues in histones is generally associated with a relaxed and permissive chromatin architecture, and therefore, indicative of positive transcriptional regulation [56]. We report that total H3Ac levels increase in cells when stimulated with LPS/IFNγ, in a cytoskeleton-dependent manner. Indeed, previous studies have demonstrated a link between inflammation and histone acetylation. Endothelial shear stress-induced inflammatory eNOS secretion is tied to enhanced p300 HAT activity at the *Nos3* promoter. Macrophages treated with HAT inhibitors, specifically curcumin [57], garcinol [58], and C646 [59], show reduced NF-κB activation and inflammatory marker expression upon stimulation. Here, we also report a decrease in global H3Ac levels in elongated macrophages.

From our network analysis, we also note an intricately connected set of genes that upregulate during LPS stimulation but whose gene expression may also be H3Ac dependent. Examining protein-level interactions between the genes of this cluster using previously reported associations through the String database, we find that the tyrosine kinase Src is at the interface of connections between the inflammatory and adhesome clusters. Src was also one of the genes whose promoter showed substantial increases in H3Ac with LPS in an iBet-sensitive manner. In addition, we also found that focal adhesions (visualized by vinculin staining), which help activate Src, were more diffuse and weaker in cells on micropatterns and those treated with iBet. This led us to explore the effect of Src knockdown and inhibition on H3Ac acetylation and find that a Src-p300 axis controls H3Ac levels in macrophages, and that this is vital for inflammatory activation. Src activation requires integrin engagement [43] and an intact cytoskeleton [60], making it highly probable that the dampened Src activity observed in cells on micropatterns are due to morphological and

adhesome modifications caused by low-adhesive culture conditions. In addition, previous studies have shown that Src activity (and consequent RhoA inactivation) is dampened within micropatterned HeLa cells [61].

In our LPS/IFNγ stimulation time course, we find that Src gets activated, and PKCδ levels transiently drop with a concomitant increase in Y311 phosphorylated PKCδ. Our experiments also show that the change in levels of PKCδ are Src-dependent. Blocking PKCδ through rottlerin also results in elevated p300 activity and H3Ac levels. Src has been previously reported to phosphorylate PKCδ at Y311 leading to its functional inactivation and degradation [45,46]. While PKCδ is a known antagonist of p300 HAT activity [35,44], our results reveal that Src activation is linked to p300 and H3 hyperacetylation through PKCδ phosphorylation and subsequent degradation during early macrophage polarization. We do note, however, that PKCδ levels rise back to pre-stimulation levels by 120 min post-stimulation, further suggesting that this transient drop in PKCδ represents a temporal window for release of p300 repression. Fig. 8 provides an illustration summarizing the Src-H3 acetylation signaling axis proposed in this study.

5. Conclusions

In summary, it has been proposed that macrophages fine-tune their immune responses, in part, through the activity of signaling molecules that function as mechanosensitive “rheostats”, which operate by effectively increasing (or deceasing) the output of certain signaling pathways. Given their demonstrated ability to both i) propagate mechanical signals from outside of the cell and ii) modulate the activity of integrin and immunoreceptor signaling pathways, Src and several Src-family member kinases have been proposed as candidate drivers of this rheostat-like behavior [62], however a clear mechanism has not been fully elucidated. At the same time, several studies have recently established that epigenetic modifications are essential for immune signal activation in macrophages, yet no studies to date have explored whether macrophages utilize epigenetic mechanisms as a means to fine-tune immune signaling output in response to biophysical cues. Here, we examined the role of epigenetic signaling in the regulation of mechanosensitive inflammatory gene activity. Our current study reveals, for the first time, a Src-histone H3 acetylation (H3Ac) signaling axis that is essential to the macrophage inflammatory response, and serves as both a modulator of immune signaling “gain” as well as an autoregulatory (negative) feedback mechanism to maintain Src expression levels during polarization. Importantly, we also observe that Src kinase activity was attenuated within low-adhesive culture conditions (where decreases in global levels of H3Ac were also noted) suggesting that Src may be largely responsible for biophysically-induced changes in histone modifications as reported by us and many others [5,22,63].

Taken together, our study highlights Src as a mediator of shape-dependent changes in H3Ac levels and inflammatory activation of macrophages. We provide first-ever evidence that Src acts as a rheostat to immune signaling activity in macrophages through a novel Src-epigenetic signaling axis. Given that Src plays multiple roles in macrophage biology, we believe our results have the potential to clarify critical regulatory mechanisms of innate immunity and greatly advance our understanding of the cell-material interface.

Supplementary Material

Refer to Web version on PubMed Central for supplementary material.

Acknowledgements

We thank Julien Morival for assistance with ChIP-Seq data analysis. We would also like to acknowledge Tim D. Smith for the custom python script that was used to analyze cell migration data, and Hamza Atcha for assistance with micropatterning.

Funding information

This work was supported by National Institutes of Health (NIH) National Institute of Allergy and Infectious Disease (NIAID) Grant R21AI128519–01 and R01AI151301-01 to W.F.L, NIH National Institute of Biomedical Imaging and Bioengineering (NIBIB) Grant R21EB027840-01 to T.L.D and W.F.L, and NIH New Innovator Award (DP2) Grant DP2CA250382-01, a National Science Foundation (NSF) grant (DMS1763272) and a grant from the Simons Foundation (594598 QN) to T.L.D. T.A.Q.P. was supported by a T32 training grant from the NIH (HL116270). This study was made possible, in part, through access to the Optical Biology Core Facility of the Developmental Biology Center, a shared resource supported by the Cancer Center Support Grant (CA-62203) and Center for Complex Biological Systems Support Grant (GM-076516) at the University of California, Irvine, and an Olympus Fluoview FV3000 confocal microscope within the Edwards Lifesciences Foundation Cardiovascular Innovation and Research Center (CIRC) supported by grant from NIH (1S10OD025064-01A1).

Data availability

The processed source data and unmodified Western blots in our figures are available as supplement files to this submission.

References

[1]. Meli VS, Veerasubramanian PK, Atcha H, Reitz Z, Downing TL, Liu WF, Biophysical regulation of macrophages in health and disease, J. Leukoc. Biol 106 (2) (2019) 283–299. [PubMed: 30861205]

[2]. Jain N, Vogel V, Spatial confinement downsizes the inflammatory response of macrophages, Nat. Mater 17 (12) (2018) 1134–1144. [PubMed: 30349032]

[3]. Mennens SFB, van den Dries K, Cambi A, Role for mechanotransduction in macrophage and dendritic cell immunobiology, in: Kloc M (Ed.), Macrophages: Origin, Functions and Biointervention, Springer International Publishing, Cham, 2017, pp. 209–242.

[4]. McWhorter FY, Wang T, Nguyen P, Chung T, Liu WF, Modulation of macrophage phenotype by cell shape, Proc. Natl. Acad. Sci. U. S. A 110 (43) (2013) 17253–17258. [PubMed: 24101477]

[5]. Meli VS, Atcha H, Veerasubramanian PK, Nagalla RR, Luu TU, Chen EY, Guerrero-Juarez CF, Yamaga K, Pandori W, Hsieh JY, Downing TL, Fruman DA, Lodoen MB, Plikus MV, Wang W, Liu WF, YAP-mediated mechanotransduction tunes the macrophage inflammatory response, Sci Adv 6 (49) (2020).

[6]. Hind LE, Dembo M, Hammer DA, Macrophage motility is driven by frontal-towing with a force magnitude dependent on substrate stiffness, Integr Biol (Camb) 7 (4) (2015) 447–453. [PubMed: 25768202]

[7]. Hind LE, Lurier EB, Dembo M, Spiller KL, Hammer DA, Effect of M1-M2 polarization on the motility and traction stresses of primary human macrophages, Cell. Mol. Bioeng 9 (3) (2016) 455–465. [PubMed: 28458726]

[8]. Chen CS, Mrksich M, Huang S, Whitesides GM, Ingber DE, Geometric control of cell life and death, Science 276 (5317) (1997) 1425–1428. [PubMed: 9162012]

[9]. Kilian KA, Bugarija B, Lahn BT, Mrksich M, Geometric cues for directing the differentiation of mesenchymal stem cells, Proc. Natl. Acad. Sci. U. S. A 107 (11) (2010) 4872–4877. [PubMed: 20194780]

[10]. McBeath R, Pirone DM, Nelson CM, Bhadriraju K, Chen CS, Cell shape, cytoskeletal tension, and RhoA regulate stem cell lineage commitment, Dev. Cell 6 (4) (2004) 483–495. [PubMed: 15068789]

[11]. D'Anselmi F, Valerio M, Cucina A, Galli L, Proietti S, Dinicola S, Pasqualato A, Manetti C, Ricci G, Giuliani A, Bizzarri M, Metabolism and cell shape in cancer: a fractal analysis, Int. J. Biochem. Cell Biol 43 (7) (2011) 1052–1058. [PubMed: 20460170]

[12]. Du E, Diez-Silva M, Kato GJ, Dao M, Suresh S, Kinetics of sickle cell biorheology and implications for painful vasoocclusive crisis, Proc. Natl. Acad. Sci. U. S. A 112 (5) (2015) 1422–1427. [PubMed: 25605910]

[13]. Wang T, Luu TU, Chen A, Khine M, Liu WF, Topographical modulation of macrophage phenotype by shrink-film multi-scale wrinkles, Biomaterials science 4 (6) (2016) 948–952. [PubMed: 27125253]

[14]. Luu TU, Gott SC, Woo BW, Rao MP, Liu WF, Micro- and nanopatterned topographical cues for regulating macrophage cell shape and phenotype, ACS Appl. Mater. Interfaces 7 (51) (2015) 28665–28672. [PubMed: 26605491]

[15]. Ivashkiv LB, Epigenetic regulation of macrophage polarization and function, Trends Immunol 34 (5) (2013) 216–223. [PubMed: 23218730]

[16]. Yang Z, Li L, Chen L, Yuan W, Dong L, Zhang Y, Wu H, Wang C, PARP-1 mediates LPS-induced HMGB1 release by macrophages through regulation of HMGB1 acetylation, J. Immunol 193 (12) (2014) 6114. [PubMed: 25392528]

[17]. Koch A, Giembycz M, Ito K, Lim S, Jazrawi E, Barnes PJ, Adcock I, Erdmann E, Chung KF, Mitogen-activated protein kinase modulation of nuclear factor-kappaB-induced granulocyte macrophage-colony-stimulating factor release from human alveolar macrophages, Am. J. Respir. Cell Mol. Biol 30 (3) (2004) 342–349. [PubMed: 12871851]

[18]. Nicodeme E, Jeffrey KL, Schaefer U, Beinke S, Dewell S, Chung CW, Chandwani R, Marazzi I, Wilson P, Coste H, White J, Kirilovsky J, Rice CM, Lora JM, Prinjha RK, Lee K, Tarakhovsky A, Suppression of inflammation by a synthetic histone mimic, Nature 468 (7327) (2010) 1119–1123. [PubMed: 21068722]

[19]. Belkina AC, Nikolajczyk BS, Denis GV, BET protein function is required for inflammation: Brd2 genetic disruption and BET inhibitor JQ1 impair mouse macrophage inflammatory responses, Journal of immunology (Baltimore, Md 190 (7) (2013) 3670–3678, 1950.

[20]. Dey A, Yang W, Gegonne A, Nishiyama A, Pan R, Yagi R, Grinberg A, Finkelman FD, Pfeifer K, Zhu J, Singer D, Zhu J, Ozato K, BRD4 directs hematopoietic stem cell development and modulates macrophage inflammatory responses, EMBO J 38 (7) (2019), e100293. [PubMed: 30842097]

[21]. Wang N, Wu R, Tang D, Kang R, The BET family in immunity and disease, Signal Transduct Target Ther 6 (1) (2021) 23. [PubMed: 33462181]

[22]. Downing TL, Soto J, Morez C, Houssin T, Fritz A, Yuan F, Chu J, Patel S, Schaffer DV, Li S, Biophysical regulation of epigenetic state and cell reprogramming, Nat. Mater 12 (12) (2013) 1154–1162. [PubMed: 24141451]

[23]. Wang P, Dreger M, Madrazo E, Williams CJ, Samaniego R, Hodson NW, Monroy F, Baena E, Sánchez-Mateos P, Hurlstone A, Redondo-Muñoz J, WDR5 modulates cell motility and morphology and controls nuclear changes induced by a 3D environment, Proc. Natl. Acad. Sci. Unit. States Am 115 (34) (2018) 8581–8586.

[24]. Schindelin J, Arganda-Carreras I, Frise E, Kaynig V, Longair M, Pietzsch T, Preibisch S, Rueden C, Saalfeld S, Schmid B, Tinevez J-Y, White DJ, Hartenstein V, Eliceiri K, Tomancak P, Cardona A, Fiji: an open-source platform for biological-image analysis, Nat. Methods 9 (7) (2012) 676–682. [PubMed: 22743772]

[25]. Tse JR, Engler AJ, Preparation of hydrogel substrates with tunable mechanical properties (Chapter 10). Current Protocols in Cell Biology, 2010. Unit 10.16.

[26]. Knoll SG, Ali MY, Saif MT, A novel method for localizing reporter fluorescent beads near the cell culture surface for traction force microscopy, JoVE : JoVE 91 (2014) 51873.

[27]. Tseng Q, Duchemin-Pelletier E, Deshiere A, Balland M, Guillou H, Filhol O, Thery M, Spatial organization of the extracellular matrix regulates cell-cell junction positioning, Proc. Natl. Acad. Sci. U. S. A 109 (5) (2012) 1506–1511. [PubMed: 22307605]

[28]. Martiel J-L, Leal A, Kurzawa L, Balland M, Wang I, Vignaud T, Tseng Q, Théry M, Chapter 15 - measurement of cell traction forces with ImageJ, in: Paluch EK (Ed.), Methods in Cell Biology, Academic Press 2015, 269–287. 10.1016/bs.mcb.2014.10.008.

[29]. Zaidel-Bar R, Itzkovitz S, Ma'ayan A, Iyengar R, Geiger B, Functional atlas of the integrin adhesome, Nat. Cell Biol 9 (8) (2007) 858–867. [PubMed: 17671451]

[30]. Zaidel-Bar R, Cadherin adhesome at a glance, J. Cell Sci 126 (2) (2013) 373. [PubMed: 23547085]

[31]. Winograd-Katz SE, Fässler R, Geiger B, Legate KR, The integrin adhesome: from genes and proteins to human disease, Nat. Rev. Mol. Cell Biol 15 (4) (2014) 273–288. [PubMed: 24651544]

[32]. Csardi G, Nepusz T, The igraph software package for complex network research, Int J Complex Syst 1695 (2006).

[33]. Szklarczyk D, Gable AL, Lyon D, Junge A, Wyder S, Huerta-Cepas J, Simonovic M, Doncheva NT, Morris JH, Bork P, Jensen LJ, Mering CV, STRING v11: protein-protein association networks with increased coverage, supporting functional discovery in genome-wide experimental datasets, Nucleic Acids Res 47 (D1) (2019) D607–d613. [PubMed: 30476243]

[34]. Tsankov AM, Gu H, Akopian V, Ziller MJ, Donaghey J, Amit I, Gnirke A, Meissner A, Transcription factor binding dynamics during human ES cell differentiation, Nature 518 (7539) (2015) 344–349. [PubMed: 25693565]

[35]. Gong J, Zhu J, Goodman OB Jr., R.G. Pestell, P.N. Schlegel, D.M. Nanus, R. Shen, Activation of p300 histone acetyltransferase activity and acetylation of the androgen receptor by bombesin in prostate cancer cells, Oncogene 25 (14) (2006) 2011–2021. [PubMed: 16434977]

[36]. Reitz ZJW, The Biophysical Micro-environment's Influence on Cell Fate Decisions during Macrophage Activation and Somatic Cell Reprogramming, eScholarship, University of California, 2019.

[37]. Williams LM, Ridley AJ, Lipopolysaccharide induces actin reorganization and tyrosine phosphorylation of Pyk2 and paxillin in monocytes and macrophages, J. Immunol 164 (4) (2000) 2028. [PubMed: 10657655]

[38]. Missirlis D, Haraszti T, Scheele C, Wiegand T, Diaz C, Neubauer S, Rechenmacher F, Kessler H, Spatz JP, Substrate engagement of integrins alpha5beta1 and alphavbeta3 is necessary, but not sufficient, for high directional persistence in migration on fibronectin, Sci. Rep 6 (2016) 23258. [PubMed: 26987342]

[39]. Hsieh JY, Keating MT, Smith TD, Meli VS, Botvinick EL, Liu WF, Matrix crosslinking enhances macrophage adhesion, migration, and inflammatory activation, APL bioengineering 3 (1) (2019), 016103. [PubMed: 31069336]

[40]. Albuschies J, Vogel V, The role of filopodia in the recognition of nanotopographies, Sci. Rep 3 (2013), 1658–1658. [PubMed: 23584574]

[41]. Rape AD, Guo WH, Wang YL, The regulation of traction force in relation to cell shape and focal adhesions, Biomaterials 32 (8) (2011) 2043–2051. [PubMed: 21163521]

[42]. Ghisletti S, Barozzi I, Mietton F, Polletti S, De Santa F, Venturini E, Gregory L, Lonie L, Chew A, Wei C-L, Ragoussis J, Natoli G, Identification and characterization of enhancers controlling the inflammatory gene expression program in macrophages, Immunity 32 (3) (2010) 317–328. [PubMed: 20206554]

[43]. Hu X, Han C, Jin J, Qin K, Zhang H, Li T, Li N, Cao X, Integrin CD11b attenuates colitis by strengthening Src-Akt pathway to polarize anti-inflammatory IL-10 expression, Sci. Rep 6 (2016) 26252. [PubMed: 27188220]

[44]. Yuan LW, Soh JW, Weinstein IB, Inhibition of histone acetyltransferase function of p300 by PKCdelta, Biochim. Biophys. Acta 1592 (2) (2002) 205–211. [PubMed: 12379484]

[45]. Blake RA, Garcia-Paramio P, Parker PJ, Courtneidge SA, Src promotes PKCdelta degradation, Cell Growth Differ 10 (4) (1999) 231–241. [PubMed: 10319993]

[46]. Kikkawa U, Matsuzaki H, Yamamoto T, Protein kinase C delta (PKC delta): activation mechanisms and functions, J. Biochem 132 (6) (2002) 831–839. [PubMed: 12473183]

[47]. Li Y, Chu JS, Kurpinski K, Li X, Bautista DM, Yang L, Sung KLP, Li S, Biophysical regulation of histone acetylation in mesenchymal stem cells, Biophys. J 100 (8) (2011) 1902–1909. [PubMed: 21504726]

[48]. Versaevel M, Grevesse T, Gabriele S, Spatial coordination between cell and nuclear shape within micropatterned endothelial cells, Nat. Commun 3 (1) (2012) 671. [PubMed: 22334074]

[49]. Arnsdorf EJ, Tummala P, Castillo AB, Zhang F, Jacobs CR, The epigenetic mechanism of mechanically induced osteogenic differentiation, J. Biomech 43 (15) (2010) 2881–2886. [PubMed: 20728889]

[50]. Le Beyec J, Xu R, Lee SY, Nelson CM, Rizki A, Alcaraz J, Bissell MJ, Cell shape regulates global histone acetylation in human mammary epithelial cells, Exp. Cell Res 313 (14) (2007) 3066–3075. [PubMed: 17524393]

[51]. Waldo SW, Li Y, Buono C, Zhao B, Billings EM, Chang J, Kruth HS, Heterogeneity of human macrophages in culture and in atherosclerotic plaques, Am. J. Pathol 172 (4) (2008) 1112–1126. [PubMed: 18321997]

[52]. Man SM, Ekpenyong A, Tourlomousis P, Achouri S, Cammarota E, Hughes K, Rizzo A, Ng G, Wright JA, Cicuta P, Guck JR, Bryant CE, Actin polymerization as a key innate immune effector mechanism to control Salmonella infection, Proc. Natl. Acad. Sci. Unit. States Am 111 (49) (2014) 17588.

[53]. Joshi H, Todd BE, Szasz T, Anaya E, Morley SC, Inflammasome activation in macrophages is regulated by actin-bundling protein L-plastin, J. Immunol 202 (1 Supplement) (2019), 117.14.

[54]. St-Pierre J, Moreau F, Cornick S, Quach J, Begum S, Aracely Fernandez L, Gorman H, Chadee K, The macrophage cytoskeleton acts as a contact sensor upon interaction with Entamoeba histolytica to trigger IL-1β secretion, PLoS Pathog 13 (8) (2017) e1006592–e1006592. [PubMed: 28837696]

[55]. Solis AG, Bielecki P, Steach HR, Sharma L, Harman CCD, Yun S, de Zoete MR, Warnock JN, To SDF, York AG, Mack M, Schwartz MA, Dela Cruz CS, Palm NW, Jackson R, Flavell RA, Mechanosensation of cyclical force by PIEZO1 is essential for innate immunity, Nature 573 (7772) (2019) 69–74. [PubMed: 31435009]

[56]. Yan C, Boyd DD, Histone H3 acetylation and H3 K4 methylation define distinct chromatin regions permissive for transgene expression, Mol. Cell Biol 26 (17) (2006) 6357–6371. [PubMed: 16914722]

[57]. Zhou Y, Zhang T, Wang X, Wei X, Chen Y, Guo L, Zhang J, Wang C, Curcumin modulates macrophage polarization through the inhibition of the toll-like receptor 4 expression and its signaling pathways, Cell. Physiol. Biochem. : international journal of experimental cellular physiology, biochemistry, and pharmacology 36 (2) (2015) 631–641.

[58]. Liao C-H, Sang S, Liang Y-C, Ho C-T, Lin J-K, Suppression of inducible nitric oxide synthase and cyclooxygenase-2 in downregulating nuclear factor-kappa B pathway by Garcinol, Mol. Carcinog 41 (3) (2004) 140–149. [PubMed: 15390082]

[59]. van den Bosch T, Boichenko A, Leus NGJ, Ourailidou ME, Wapenaar H, Rotili D, Mai A, Imhof A, Bischoff R, Haisma HJ, Dekker FJ, The histone acetyltransferase p300 inhibitor C646 reduces pro-inflammatory gene expression and inhibits histone deacetylases, Biochem. Pharmacol 102 (2016) 130–140. [PubMed: 26718586]

[60]. Na S, Collin O, Chowdhury F, Tay B, Ouyang M, Wang Y, Wang N, Rapid signal transduction in living cells is a unique feature of mechanotransduction, Proc. Natl. Acad. Sci. U. S. A 105 (18) (2008) 6626–6631. [PubMed: 18456839]

[61]. Kim TJ, Xu J, Dong R, Lu S, Nuzzo R, Wang Y, Visualizing the effect of microenvironment on the spatiotemporal RhoA and Src activities in living cells by FRET, Small 5 (12) (2009) 1453–1459. [PubMed: 19334011]

[62]. Lowell C, Src-family kinases: rheostats of immune cell signaling, Mol. Immunol 41 6–7 (2004) 631–643. [PubMed: 15220000]

[63]. Jain N, Iyer KV, Kumar A, Shivashankar GV, Cell geometric constraints induce modular gene-expression patterns via redistribution of HDAC3 regulated by actomyosin contractility, Proc. Natl. Acad. Sci. Unit. States Am 110 (28) (2013) 11349–11354.

[64]. Byeon SE, Yi Y-S, Oh J, Yoo BC, Hong S, Cho JY, The role of Src kinase in macrophage-mediated inflammatory responses, Mediat. Inflamm 2012 (2012) 512926.

[65]. Arthur WT, Petch LA, Burridge K, Integrin engagement suppresses RhoA activity via a c-Src-dependent mechanism, Curr. Biol. : CB 10 (12) (2000) 719–722. [PubMed: 10873807]

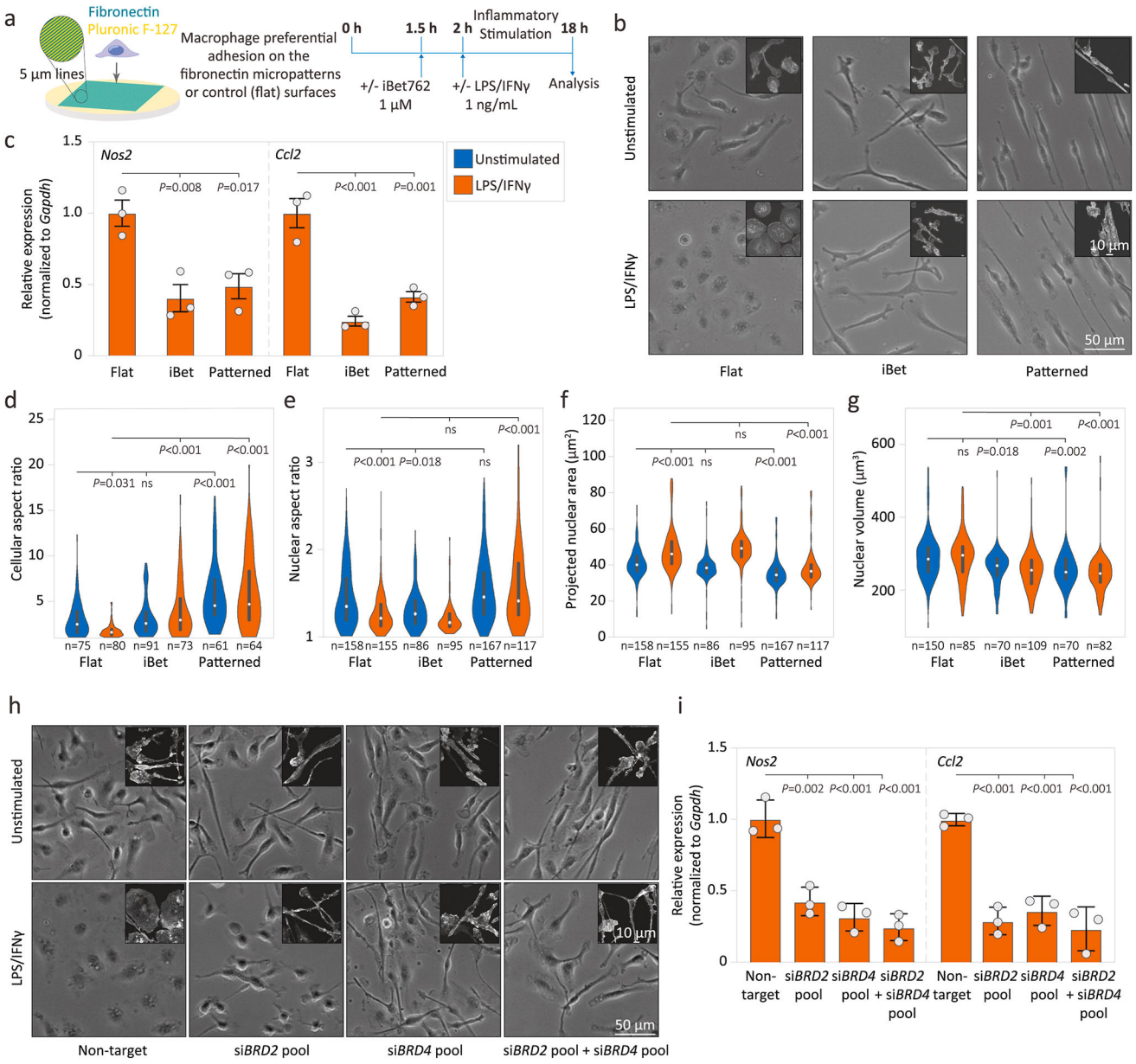

Fig. 1. Macrophages exhibit altered morphology and inflammatory activation with BET inhibition and facilitated elongation.

(a) Schematic for the micropatterning technique used to generate the 5 μm fibronectin lines, and timeline of experiments describing the experimental workflow. (b) Morphology of unstimulated and stimulated BMDMs on flats, flats with iBet and micropatterned lines, with F-actin stained in the inset figures. (c) Relative gene expression of M1 marker genes *Nos2*, and *Ccl2* in cells stimulated with LPS/IFNγ for 16 h, on the flats, flats with iBet and micropatterned conditions. Gene expression have been individually normalized to *Gapdh*. Quantification of cellular (d) and nuclear (e) aspect ratios for the BMDMs on flats, flats with iBet and micropatterned lines, and corresponding nuclear area (f), and nuclear volume (g). (h) Morphology of cells treated with siRNA against *BRD2* and *BRD4* for 3 days, and stimulated with 1 ng/ml LPS/IFNγ for 16 h. F-actin has been stained in the inset

figures. (i) Relative gene expression of M1 marker genes *Nos2*, and *Ccl2* in cells stimulated for 16 h with 1 ng/ml LPS/IFNγ, after treatment with si*BRD2* and si*BRD4* for 3 days. Gene expression have been individually normalized to *Gapdh*. Data in all panels have been represented as mean ± SEM. One-way ANOVA with multiple comparisons using Tukey test was performed. Violin plots show quartiles and median. Source data are provided.

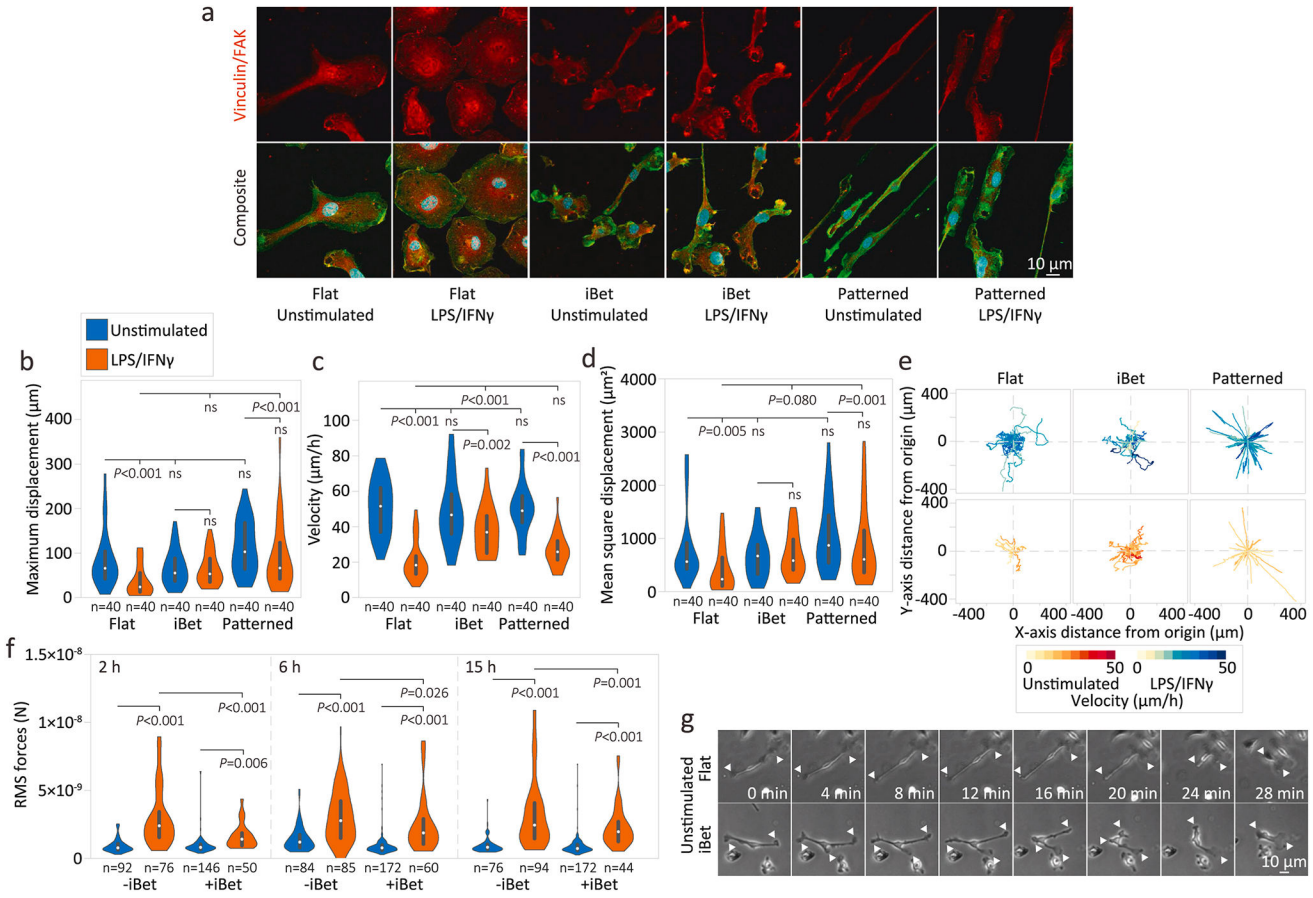

Fig. 2. Macrophages exhibit altered adhesive structures and motility with BET inhibition and facilitated elongation.

(a) Vinculin staining of unstimulated and 1 ng/ml LPS/IFNγ stimulated BMDMs on flats, flats with iBet and micropatterned lines at 16 h post stimulation. Quantifications of maximum displacement (b), velocity (c), and mean square displacements (d) for BMDMs tracked for 12 h post stimulation, and displacement rose-plots (e) for the cells on flats, flats with iBet and micropatterns, with and without LPS/IFNγ stimulation. (f) Root-mean-squared (RMS) traction forces measured at 2 h, 6 h and 15 h post stimulation, via traction force microscopy show an increase in forces with inflammatory activation that is subdued with iBet treatment. (g) Time-lapse microscopy figures demonstrating the motility behaviors of a representative macrophage on flats with and without iBet treatment; arrows point to leading-edge like protrusions that were transient and numerous (>2) in iBet-treated cells. Data in all panels have been represented as mean ± SEM. One-way ANOVA with multiple comparisons using Tukey test was performed. Violin plots show quartiles and median. Source data are provided.

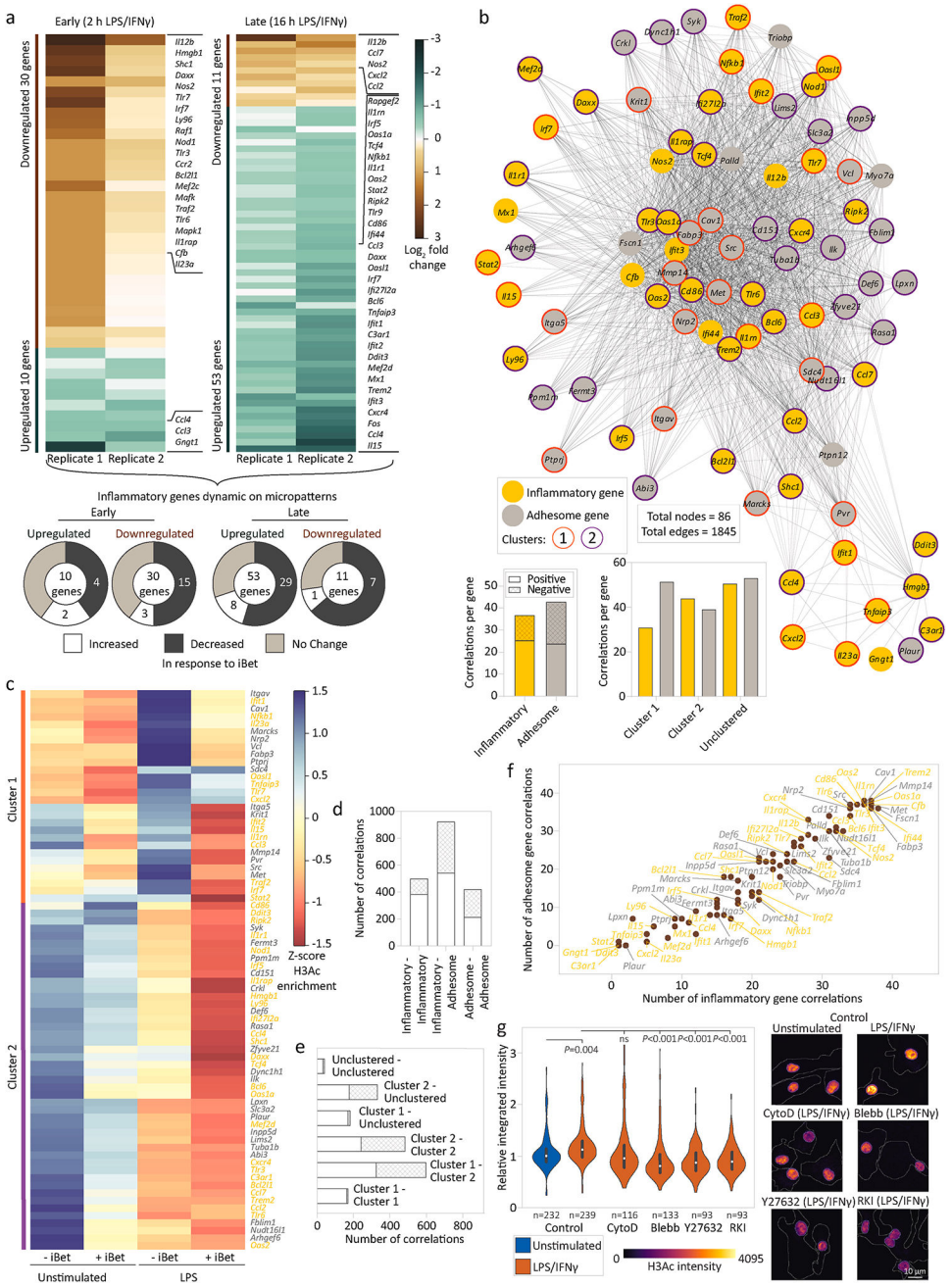

Fig. 3. Inflammatory and cell adhesion genes are co-regulated during macrophage stimulation and associate with dynamic histone acetylation.

(a) Heat map of dynamic inflammatory genes being differentially regulated with facilitated elongation (consistent across two biological replicates), at both early and late inflammatory states, and donut charts showing overlap between genes regulated with iBet treatment. (b) Gene coregulation network built with elongation-regulated differentially-expressed inflammatory genes (dynamic genes from a), and LPS-sensitive adhesome genes, and the correlations per gene for the various categories of genes in the network. (c) Heatmap showing differentially enriched H3Ac at promoter regions of the networked genes reveals a highly dynamic H3Ac landscape at 1 h post stimulation. (d) Statistics of correlations

within the network show that the dynamic adhesome and inflammatory genes are highly coregulated upon LPS stimulation. (e) Intercluster statistics that reveal that intra-cluster 1 correlations were highly positive. (f) Statistical of genes in the network, plotting them based on the number of number of correlations. (g) Immunofluorescence images and H3Ac quantifications in macrophages treated with cytoskeletal inhibitor drugs - cytochalasin-D (10 μM), blebbistatin (30 μM), Y27632 (30 μM) and RKI-1447 (10 μM), showing a reduced bulk H3Ac levels in LPS/IFNγ-activated cells. Cytoskeletal inhibitors were added 30 min prior to cytokine addition, and the cells were stained at 16 h post stimulation. p-values displayed are from one-way ANOVA with multiple comparisons using Tukey test. Violin plots show quartiles and median. Source data are provided.

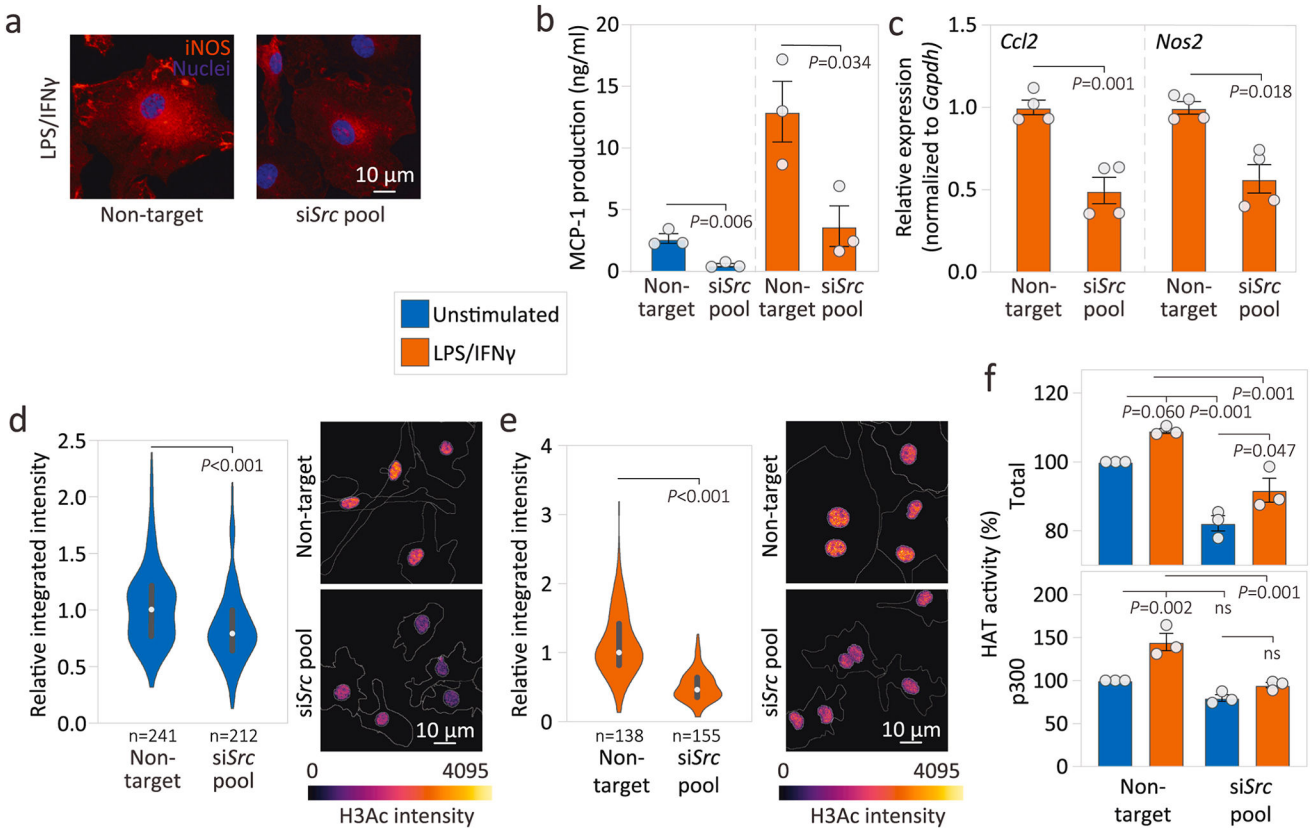

Fig. 4. Src controls H3 hyperacetylation upon LPS/IFNγ stimulation through p300.

iNOS expression (a), MCP-1 production (b), and *Nos2* and *Ccl2* gene expression levels (c) at 16 h post 1 ng/ml LPS/IFNγ stimulation in si*Src*-treated cells portray Src as an inflammatory gene. Histone acetylation staining in cells treated with si*Src* for 48 h (d), and a further 16 h of 1 ng/ml LPS/IFNγ stimulation (e) show lower global H3Ac levels with *Src* knockdown. (f) Total HAT and p300 HAT activity measured in si*Src*-treated cells 2 h post LPS/IFNγ stimulation show lower p300 HAT activity. Data has been represented as mean ± SEM, and one-way ANOVA with multiple comparisons using Tukey test was performed. Exceptions in panels b–e where only 2 conditions are available were instead subjected to Student's t-test for analysis. Violin plots show quartiles and median. Source data are provided.

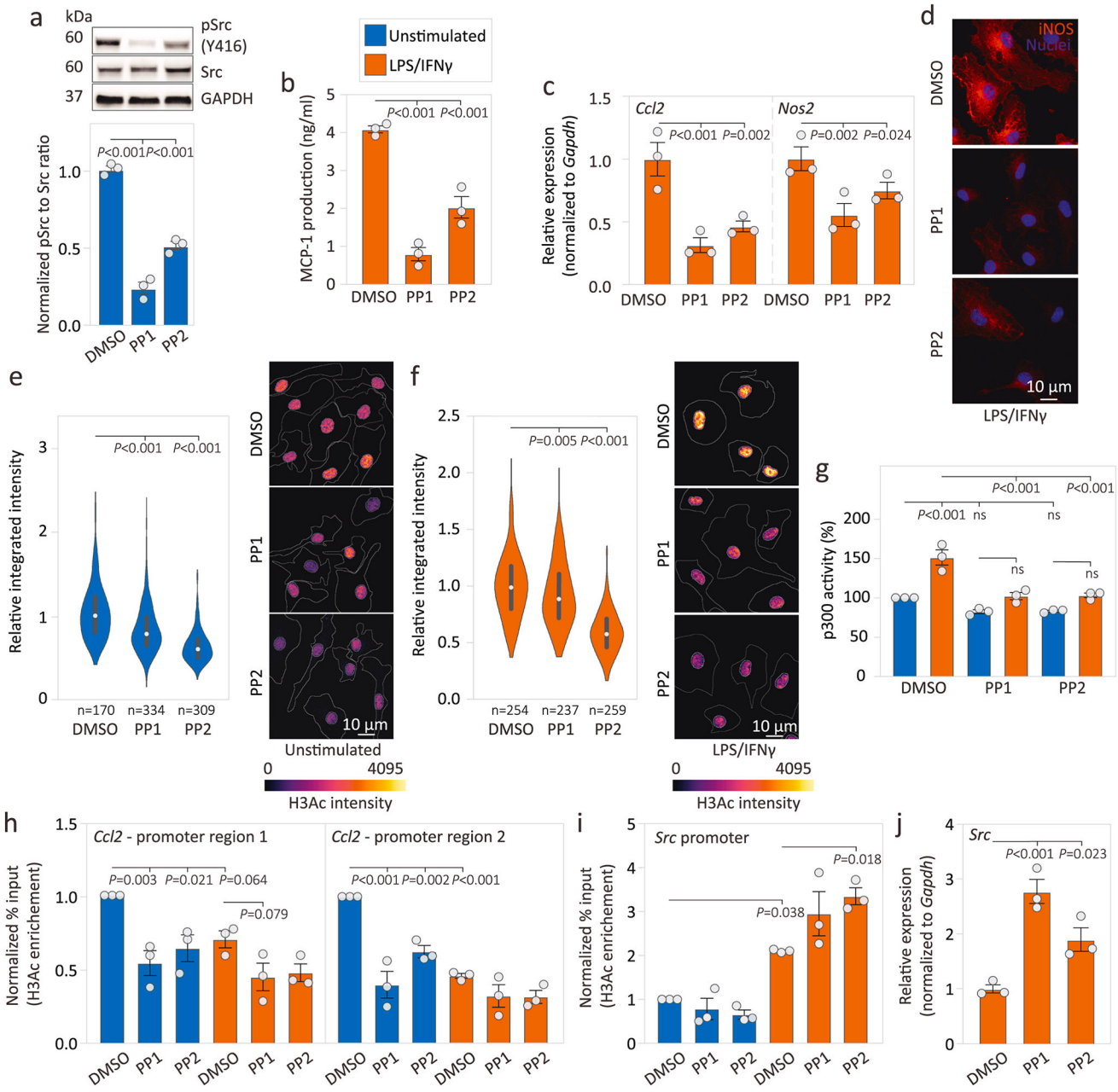

Fig. 5. Src activation drives H3 hyperacetylation through p300.

(a) Effects of PP1 (5 μM) and PP2 (5 μM) treatment on Src activation measured by Western blot. Anti-inflammatory effects of PP1 and PP2 treatments demonstrated by MCP-1 production (b), *Ccl2* and *Nos2* gene levels (c), and iNOS staining (d) in cells treated with Src inhibitors for 6 h, followed by stimulation of 1 ng/ml LPS/IFNγ for 16 h. Global H3Ac levels in cells treated with PP1 and PP2 for 24 h (e), and 6 h Src inhibitors followed by 16 h 1 ng/ml LPS/IFNγ treatment (f) show Src inhibition suppress H3Ac expression. (g) p300 activity in unstimulated and stimulated cells wherein 6 h drug treatment was followed by 2 h of 1 ng/ml LPS/IFNγ treatment show suppressed p300 activity in PP1- and PP2-treated cells. (h) *Ccl2* proximal promoter H3Ac enrichment measured at two different

loci in 6 h PP1- and PP2-treated cells that were subsequently stimulated for 2 h with 1 ng/ml LPS/IFNγ; ChIP-qPCR with pre-immune IgG displayed background signal and was comparable across conditions (data not shown). (i) *Src* proximal promoter H3Ac enrichment measured in 6 h PP1- and PP2-treated cells that were subsequently stimulated for 2 h with 1 ng/ml LPS/IFNγ. (j) *Src* gene expression in in 6 h PP1- and PP2-treated cells that were subsequently stimulated for 16 h with 1 ng/ml LPS/IFNγ. Data has been represented as mean ± SEM, and one-way ANOVA with multiple comparisons using Tukey test was performed. Violin plots show quartiles and median. Source data and unprocessed blots are provided.

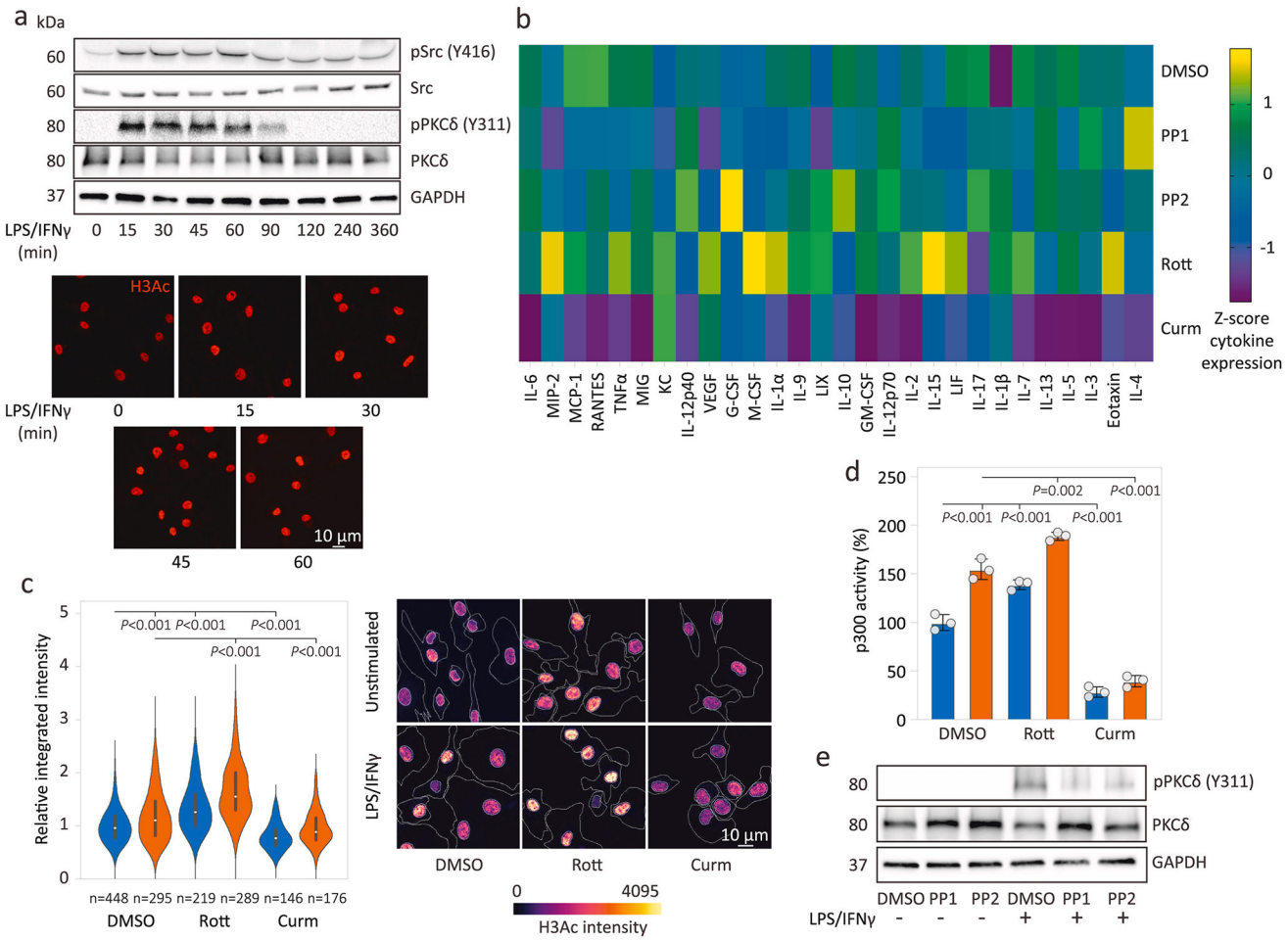

Fig. 6. LPS/IFNγ stimulation triggers Src activation and suppresses PKCδ, increasing H3Ac through derepression of p300 HAT activity.

(a) Stimulation time course with 10 ng/ml LPS/IFNγ drives up Src activity, and histone acetylation levels, along with transient drops in total PKCδ and a brief increase in Y311 phospho-PKCδ. (b) Cytokine prolife of cells treated for 6 h with inhibitory drugs that suppress Src, PKCδ and p300 activity, before stimulation with 1 ng/ml LPS/IFNγ for 16 h. Cytokines in the heatmap are ordered by the concentration observed (IL-6 being the highest). (c) Histone acetylation staining in cells treated for 6 h with rottlerin (5 μM) and curcumin (30 μM), and 16 h of 1 ng/ml LPS/IFNγ stimulation. (d) p300 HAT activity shoots up with rottlerin treatment and diminishes with curcumin addition. (e) Levels of total and Y311 phospho-PKCδ in cells treated for 6 h with PP1 (5 μM) and PP2 (5 μM), 1 h after 1 ng/ml LPS/IFNγ stimulation. Data has been represented as mean ± SEM. One-way ANOVA with multiple comparisons using Tukey test was performed. Violin plots show quartiles and median. Source data and unprocessed blots are provided.

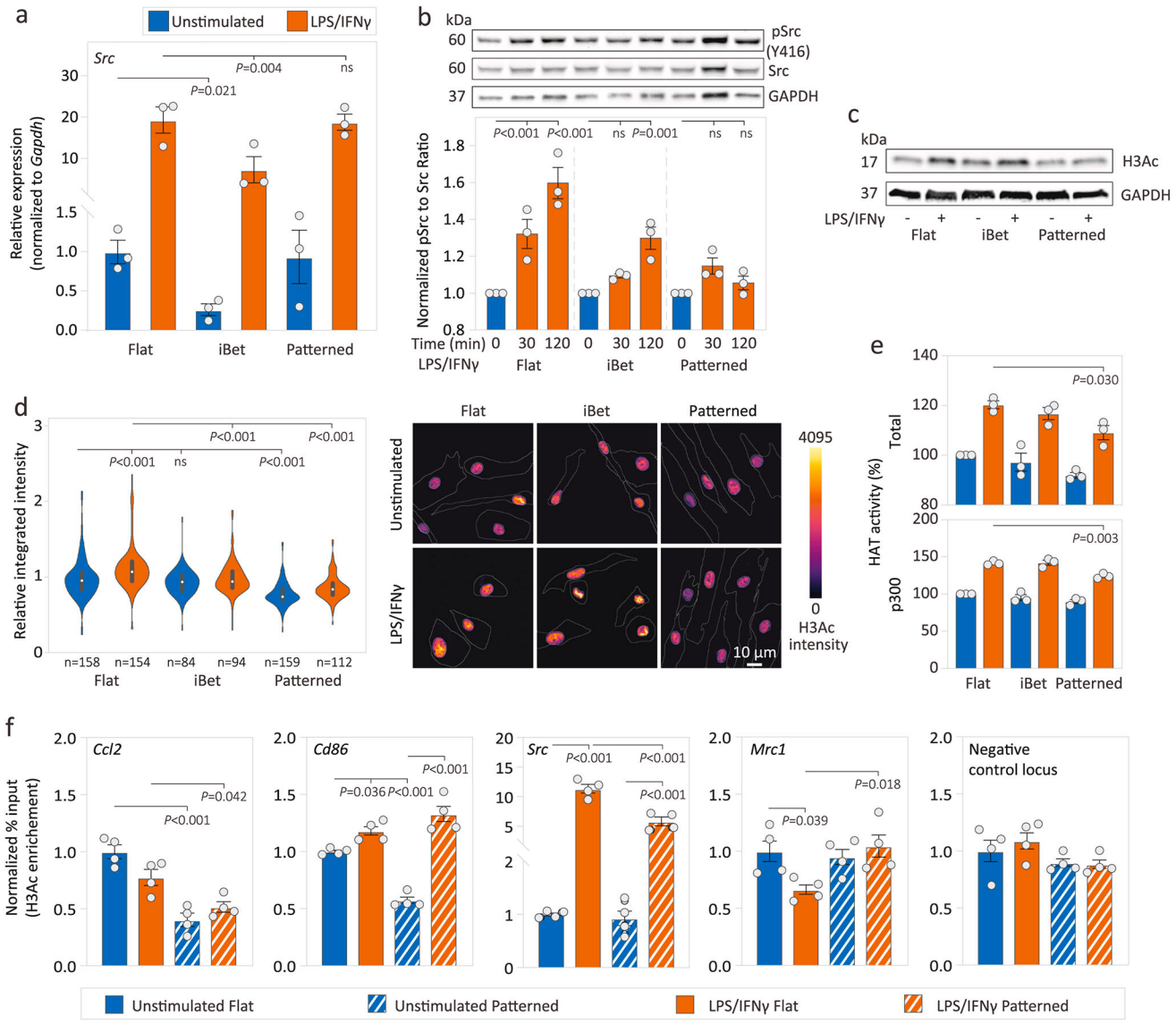

Fig. 7. Macrophage cell elongation reduces global and local histone acetylation.

(a) *Src* gene expression in cells with iBet treatment and micropatterning, 16 h post LPS/IFNγ stimulation. (b) Western blot analysis of Src activation in cells with iBet treatment and micropatterning, 30 min and 120 min post LPS/IFNγ stimulation. (c) Western blots of macrophages showing reduced bulk H3Ac levels on micropatterned surfaces at 16 h post LPS/IFNγ stimulation. (d) Immunofluorescence images and corresponding quantifications of macrophages in same conditions. (e) Total and p300 HAT activity measured in cells with iBet treatment and micropatterning. (f) ChIP-qPCR showing reduced H3Ac enrichment on the proximal promoters of inflammatory genes *Ccl2*, *Src*, and *Cd86* with facilitated elongation on micropatterns; ChIP-qPCR with pre-immune IgG displayed background signal and was comparable across conditions (data not shown). Data has been represented as mean ± SEM. One-way ANOVA with multiple comparisons using Tukey test was performed. Violin plots show quartiles and median. Source data and unprocessed blots are provided.

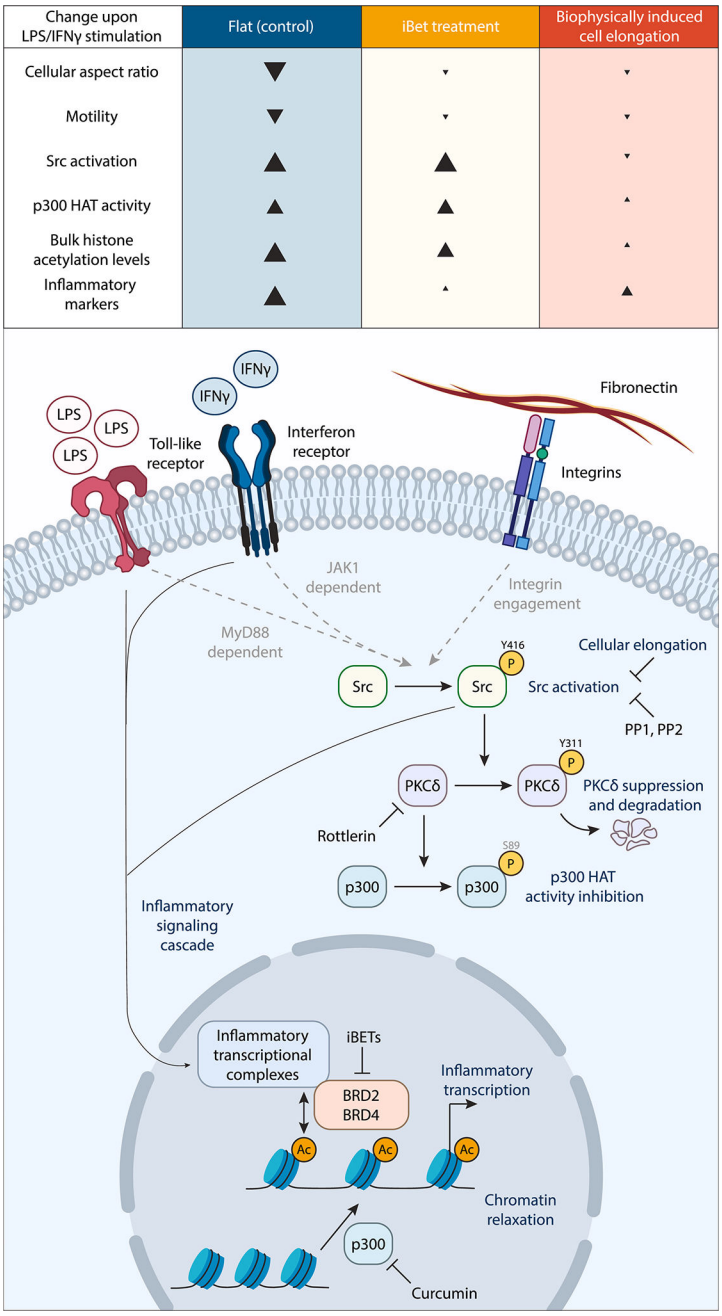

Fig. 8. Summary illustration of Src-H3 acetylation signaling axis in macrophages.

(Top) Summary of observations on cell morphology, motility, Src and p300 activity, histone acetylation levels and inflammatory activation, in cells treated with iBet or undergoing facilitated elongation. The relative impact of each condition on a given cell characteristic is conveyed through the direction (up or down) and size of arrowheads. (Bottom) Schematic portraying the cytoskeleton-epigenetic nexus that modulate inflammation in macrophages experiencing elongation or pharmacological perturbation (gray dashed arrows indicate previously reported mechanisms). Src activation is achieved by both exposure to biochemical/soluble cues such as LPS (through a MyD88-dependent mechanism) [64]

and IFNγ (through a JAK1 dependent mechanism), and biomechanical events such as ECM-integrin engagement [65]. Src activation drives PKCδ degradation and suppression by phosphorylation at Y311. Src inhibitors such as PP1 and PP2 prevent the activation of this signaling cascade. PKCδ activity suppresses p300 HAT activity by phosphorylation at S89 [44]. We show that cellular elongation can suppress Src activation even in the presence of LPS/IFNγ stimulation. This eventually leads to a diminished p300 HAT activity in elongated cells. p300 acetylates his-tones, allowing transcriptional complex binding to the chromatin. A diminished p300 activity in elongated cells thus lowers transcriptional activity of inflammatory genes. In contrast, the anti-inflammatory activity of iBets stems from their inhibition of BET family proteins (e.g., Brd2 and Brd4) that facilitate transcription factor and elongation factor binding to the chromatin. This work demonstrates a novel mechanism through which biophysical cues from the microenvironment can regulate transcriptional programs such as inflammation by rapidly modifying histones. Notably, these biophysically-induced effects can be on par with those observed through treatments with soluble pharmacological agents.